ERDC/CHL TR-08-X

Coastal and Hydraulics Laboratory

US Army Corps of Engineers®
Engineer Research and Development Center

DRAFT

Seabrook and Borgne Alignment Construction Sequence Hydrodynamic Study

Jennifer N. Tate and Cassandra G. Ross

July 2009

DRAFT

Approved for public release; distribution is unlimited.

ERDC/CHL TR-08-X
July 2009

Seabrook Fish Larval Transport Study

Jennifer N. Tate and Cassandra G. Ross

Coastal and Hydraulics Laboratory
U.S. Army Engineer Research and Development Center
3909 Halls Ferry Road
Vicksburg, MS 39180-6199

Technical report

Approved for public release; distribution is unlimited.

DRAFT

Prepared for U.S. Army Corps of Engineers, New Orleans District, Hurricane Protection Office

Contents

Figures iii

Preface v

Unit Conversion Factors vi

1 Introduction 7

Background 7
Technical Approach 9

2 Model Development 11

Model Description 11
Mesh Development 12
Boundary Conditions 13

3 Construction Sequence Plans 15

4 Hydrodynamic Results 23

Velocity Magnitudes 23
Water Surface Analysis 37
Circulation Changes 56

5 Conclusions 58

References 60

Appendix: Description of the Adaptive Hydraulics Model (ADH) 61

DRAFT

Figures

Figure 1-1. Vicinity map 8
Figure 1-2. Project area map 9
Figure 2-1. Model domain and bathymetry 13
Figure 2-2. Location of river inflows 14
Figure 3-1. Base configuration: no closures, no structures 16
Figure 3-2. Plan 1 configuration: close the MRGO at La Loutre 17
Figure 3-3. Plan 2 configuration: includes Plan 1 and the Borgne alignment (56 ft X 8 ft gate on Bayou Bienvenue, and two 150 ft X 16 ft gates on GIWW) 18
Figure 3-4. February 2010 configuration: close the MRGO at La Loutre, close the MRGO south of Bayou Bienvenue, cofferdam at the Bayou Bienvenue gate, cofferdam at the sector gate on GIWW, and open the 150 ft X 16 ft barge gate on GIWW 19
Figure 3-5. March 2010 configuration: includes February 2010 configuration with a cofferdam at the Seabrook structure as well 20
Figure 3-6. Tide signal for the September analysis period 21
Figure 3-7. Tide signal for the March analysis period 21
Figure 3-8. Wind signal for the September analysis period 22
Figure 3-9. Wind signal for the March analysis period 22
Figure 4-1. Hydrodynamic analysis locations - Seabrook 23
Figure 4-2. Hydrodynamic analysis locations – Bayou Bienvenue Structure, GIWW Sector Gate, and GIWW Barge Gate 24
Figure 4-3. Hydrodynamic analysis locations – Chef Menteur and Rigolets 24
Figure 4-4. Velocity average for September (positive) 25
Figure 4-5. Velocity average for September (negative) 26
Figure 4-6. Velocity maximum for September (positive) 26
Figure 4-7. Velocity minimum for September (negative) 27
Figure 4-8. Velocity average for March (positive) 27
Figure 4-9. Velocity average for March (negative) 28
Figure 4-10. Velocity maximum for March (positive) 28
Figure 4-11. Velocity minimum for March (negative) 29
Figure 4-12. Percent exceedance of velocity magnitude analysis locations 30
Figure 4-13. GIWW Barge Gate percent exceedance plot for September 31
Figure 4-14. Location map for water surface analysis 38
Figure 4-15. Inset for water surface analysis location map 38
Figure 4-16. Water surface elevation north of MRGO closure at La Loutre (September) 39
Figure 4-17. Water surface elevation south of MRGO closure at La Loutre (September) 39
Figure 4-18. Water surface elevation north of MRGO closure at Bayou Bienvenue (September) 40

DRAFT

Figure 4-19. Water surface elevation south of MRGO closure at Bayou Bienvenue (September) 40
Figure 4-20. Water surface elevation west of Bayou Bienvenue structure (September) 41
Figure 4-21. Water surface elevation east of Bayou Bienvenue structure (September) 41
Figure 4-22. Water surface elevation west of GIWW structures (September) 42
Figure 4-23. Water surface elevation east of GIWW structures (September) 42
Figure 4-24. Water surface elevation north of Seabrook structure (September) 43
Figure 4-25. Water surface elevation south of Seabrook structure (September) 43
Figure 4-26. Water surface elevation in GIWW at IHNC (September) 44
Figure 4-27. Water surface elevation in Chef Menteur (September) 44
Figure 4-28. Water surface elevation north in Rigolets (September) 45
Figure 4-29. Water surface elevation at Lake Borgne perimeter (September) 45
Figure 4-30. Water surface elevation at Lake Borgne center (September) 46
Figure 4-31. Water surface elevation at Lake Pontchartrain (September) 46
Figure 4-32. Water surface elevation north of MRGO closure at La Loutre (March) 47
Figure 4-33. Water surface elevation south of MRGO closure at La Loutre (March) 47
Figure 4-34. Water surface elevation north of MRGO closure at Bayou Bienvenue (March) 48
Figure 4-35. Water surface elevation south of MRGO closure at Bayou Bienvenue (March) 48
Figure 4-36. Water surface elevation west of Bayou Bienvenue structure (March) 49
Figure 4-37. Water surface elevation east of Bayou Bienvenue structure (March) 49
Figure 4-38. Water surface elevation west of GIWW structures (March) 50
Figure 4-39. Water surface elevation east of GIWW structures (March) 50
Figure 4-40. Water surface elevation north of Seabrook structure (March) 51
Figure 4-41. Water surface elevation south of MRGO Seabrook structure (March) 51
Figure 4-42. Water surface elevation in GIWW at IHNC (March) 52
Figure 4-43. Water surface elevation in Chef Menteur (March) 52
Figure 4-44. Water surface elevation in Rigolets (March) 53
Figure 4-45. Water surface elevation at Lake Borgne perimeter (March) 53
Figure 4-46. Water surface elevation at Lake Borgne center (March) 54
Figure 4-47. Water surface elevation in Lake Pontchartrain (March) 54
Figure 4-48. February 2010 plan circulation 57
Figure 4-49. March 2010 plan circulation 57

DRAFT

Preface

The model investigation presented in this report was authorized and funded by the U.S. Army Corps of Engineers Hurricane Protection Office (HPO), New Orleans in an effort to support the navigation impacts analysis modeling of the proposed construction sequence for hurricane protection structures along the Gulf Intracoastal Waterway and Inner Harbor Navigation Canal. This work was performed in conjunction with the environmental impacts analysis modeling effort which will be documented in Individual Environmental Report #11 Tier 2 Pontchartrain for the improved protection of the Inner Harbor Navigation Canal. This work was conducted by Ms. Jennifer Tate and Ms. Cassandra Ross.

This work was conducted at the Coastal and Hydraulics Laboratory (CHL) of the U. S. Army Engineer Research and Development Center (ERDC) during the period of June 2009 to July 2009 under the direction of William Martin, Director of the CHL; Mr. Bruce Ebersole, Chief of the Flood Protection Division, CHL; Dr. Robert T. McAdory, Chief of the Estuarine Engineering Branch, CHL.

Dr. James R. Houston was Director of ERDC. COL Gary Johnston was Commander and Executive Director.

DRAFT

Unit Conversion Factors

Multiply	By	To Obtain
acres	4,046.873	square meters
acre-feet	1,233.5	cubic meters
cubic feet	0.02831685	cubic meters
cubic inches	1.6387064 E-05	cubic meters
cubic yards	0.7645549	cubic meters
degrees (angle)	0.01745329	radians
degrees Fahrenheit	(F-32)/1.8	degrees Celsius
fathoms	1.8288	meters
feet	0.3048	meters
foot-pounds force	1.355818	joules
inches	0.0254	meters
inch-pounds (force)	0.1129848	newton meters
knots	0.5144444	meters per second
microns	1.0 E-06	meters
miles (nautical)	1,852	meters
miles (U.S. statute)	1,609.347	meters
slugs	14.59390	kilograms
square feet	0.09290304	square meters
square yards	0.8361274	square meters
yards	0.9144	meters

DRAFT

1 Introduction

Background

The U. S. Army Corps of Engineers Hurricane Protection Office (HPO) is authorized to provide New Orleans with a 100 year hurricane and storm damage risk reduction system (HSDRRS). The purpose and need for the proposed action is to provide, in a timely manner, the 100-year level of risk reduction from flood damage to the areas surrounding the IHNC due to flooding from hurricanes and other severe storm events. The term "100-year level of risk reduction" as it is used here refers to a level of risk reduction that reduces the risk of storm surge and wave-driven flooding that the New Orleans Metropolitan Area has a one percent chance of experiencing in any given year. The proposed action resulted from a defined need to reduce flood risk and storm damage to residences, businesses, and other infrastructure from hurricanes (100-year storm events), and other high water events. The completed HSDRRS would lower the risk of harm to citizens and damage to infrastructure during a storm event.

This risk reduction is being accomplished through the construction of a comprehensive system of levees, gates, and drainage structures. Several planned structures (to be located along the levee system) allow for continued navigation in the Inner Harbor Navigational Canal (IHNC), Bayou Bienvenue, and the Gulf Intracoastal Waterway (GIWW). The IHNC Seabrook, Bayou Bienvenue, and GIWW gate structures are designed to remain open during normal tidal conditions with the ability to close during surge events, however, navigation results may require a change in the operation procedures.

HPO requested that the USACE Engineer Research and Development Center (ERDC) at Waterways Experiment Station perform a numerical modeling study for the purpose of analyzing the temporary construction impacts of proposed HSDRRS measures to be placed in the Gulf Intracoastal Waterway (GIWW) and the Mississippi River Gulf Outlet (MRGO). This study was requested in addition to separate environmental studies on the impacts to fish larval transport and navigation studies to analyze the impacts the protection measures have on the hydrodynamics and vessel traffic. Figure 1-1 shows the project vicinity. Figure 1-2 shows a more detailed project area.

DRAFT

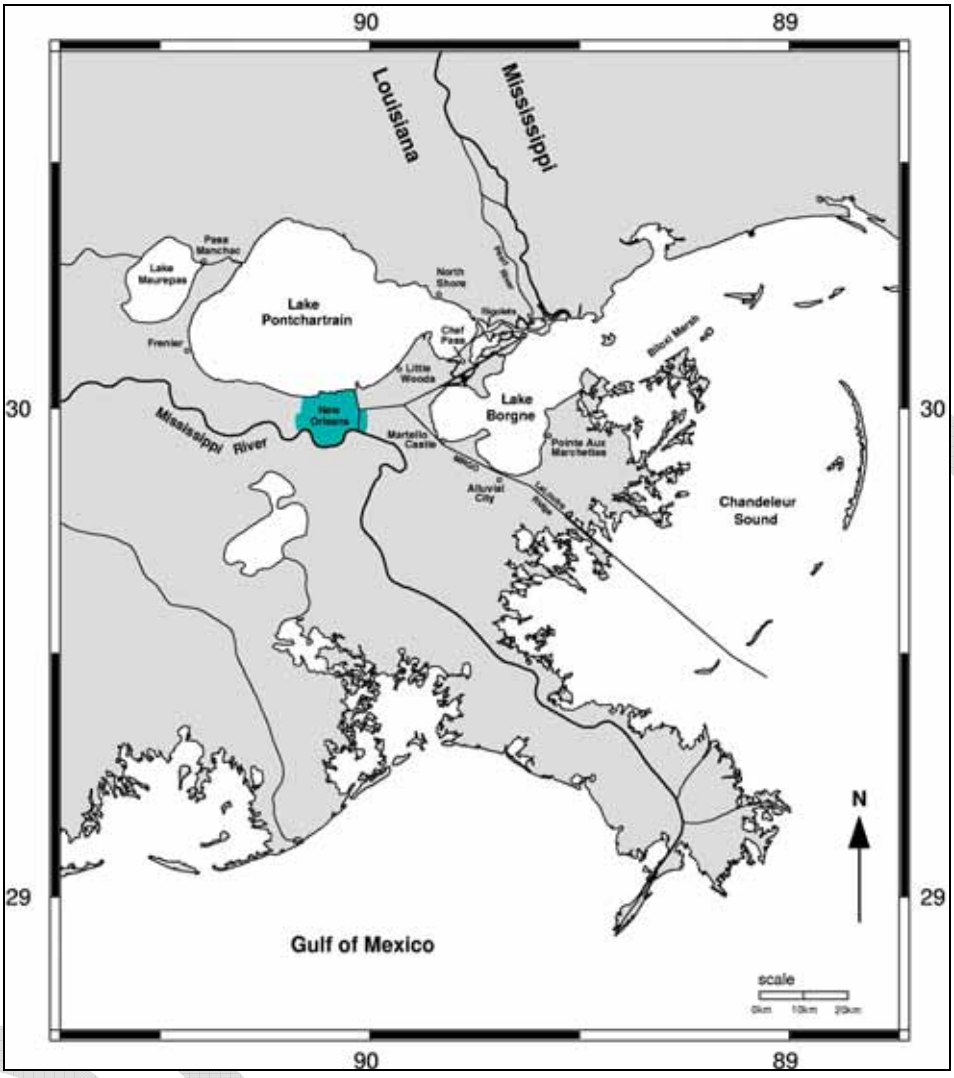

Figure 1-1. Vicinity map

Figure 1-2. Project area map

The MRGO Canal is a 66-mile-long deepwater channel that extends northwest from deep water in the Gulf of Mexico to New Orleans, LA. The MRGO merges with the GIWW and continues 5 miles further to the west where it joins the Inner Harbor Navigation Canal (IHNC). The IHNC continues approximately another 3 miles north from its intersection with the GIWW to connect with Lake Pontchartrain at Seabrook. To the East of the connection of the GIWW with the MRGO, the GIWW extends northeast approximately 6 miles to its first connection with Lake Borgne and 20 miles to its connection to the Rigolets, located to the northeast of Chef Menteur beyond the extents of Figure 1-2.

Technical Approach

The modeling for this study considers hydrodynamic movement using the shallow water module of the ADH code in two-dimensions. The modeling effort presented in this document is continued from the effort performed in Tate et al. 2009. Details of the model development, mesh characteristics, boundary condition generation, and model validation are found in the

2009 report. Since this specific work concerns the construction sequence of the protection measures, a structure is either open or closed for the entire time of a simulation. The results of these simulations will be compared to results for a plan in which no changes are made to the system, a plan in which the MRGO is cut off at La Loutre, and a plan in which the MRGO is cut off at La Loutre and the Borgne alignment is in place. Further details of the conditions used for simulation and comparison will be provided in Chapter 3.

The time periods for simulation and analysis are the same as those presented in Tate et al. 2009. Two different four-week periods are simulated as specified by HPO. The periods included for these simulations are August 15 – September 15, 2007 and March 1-31, 2008.

DRAFT

2 Model Development

Hydrodynamic Numerical Model

The hydrodynamic code used in this study is Adaptive Hydraulics (ADH). ADH is a finite element code that can simulate three-dimensional groundwater, three-dimensional navier-stokes, and two- and three-dimensional shallow water equations. This study utilizes the 2-dimensional shallow water equations of ADH. The model is simulated on high performance computing machines in order to obtain quick results. Further details on the ADH model and its equations can be found in Appendix A and several publications are available at https://adh.usace.army.mil.

The model is validated with field data from 2008 of water surface elevation, discharge, and velocity. Current bathymetry data was collected by ERDC-CHL in the IHNC, GIWW, and northern MRGO to approximately channel mile 56. The model boundary conditions include the tidal boundary, river inflows, and wind forcings. Details of the model validation can be found in Tate et al. 2009, including boundary condition development and comparison of model results to the available field data.

Model Description

Adaptive Hydraulics (ADH) is the modeling tool used for the simulations in this study. ADH is a finite element model that is capable of simulating three-dimensional Navier Stokes equations, two and three-dimensional shallow water equations, and groundwater equations. It can be used in a serial or multiprocessor mode on personal computers, UNIX, Silicon Graphics, and CRAY operating systems. The uniqueness of ADH is its ability to dynamically refine the domain mesh in areas where more resolution is needed at certain times due to changes in the flow conditions. ADH can simulate the transport of conservative constituents, such as dye clouds, as well as sediment transport that is coupled to bed and hydrodynamic changes. The ability of ADH to allow the domain to wet and dry within the marsh areas as the tide changes is suitable for the shallow marsh environment present in a few locations included in the model domain. This tool is

DRAFT

being developed at CHL and has been used to model sediment transport in sections of the Mississippi River, tidal conditions in southern California, and vessel traffic in the Houston Ship Channel.

For this study, the two-dimensional shallow water module of ADH will be used for all simulations. This tool solves for depth and depth averaged velocity throughout the model domain. In this case, density effects due to salinity or other factors are being ignored and therefore their effects on the flow are not included in these simulations and results. More details of the two-dimensional shallow water module of ADH and its computational philosophy and equations can be found in Appendix A or at https://adh.usace.army.mil.

Mesh Development

The computational model domain is given in Figure 2-1. This is the same model domain as in previous studies of this area as described in McAnally et al. 1997 and Tate et al. 2002. This mesh has since been modified to include more recent bathymetry and additional marsh storage and flow pathways for the navigation study of the Borgne alignment. The domain extends east of the Chandeleur Islands in the Gulf of Mexico, follows the coastline of Mississippi and Louisiana on the north, follows the MRGO on the south, and includes Lake Pontchartrain and Lake Maurepas. The actual mesh was taken from that used in the navigation study and modified to fit the ADH format of linear, triangular elements. Bathymetry data was collected by ERDC-CHL in the IHNC, GIWW, Bayou Bienvenue and northern MRGO in November 2008. This data were incorporated into the mesh. Mesh boundaries were also better defined along the IHNC, GIWW, and Bayou Bienvenue. The vertical datum for this mesh is NAVD 88 (2004.65). This Base mesh is identical to that used for the hydrodynamic modeling and particle tracking simulations as documented in Tate et al. 2009. The model validation is also included in the referenced document. From the Base mesh, the requested plan conditions are incorporated.

DRAFT

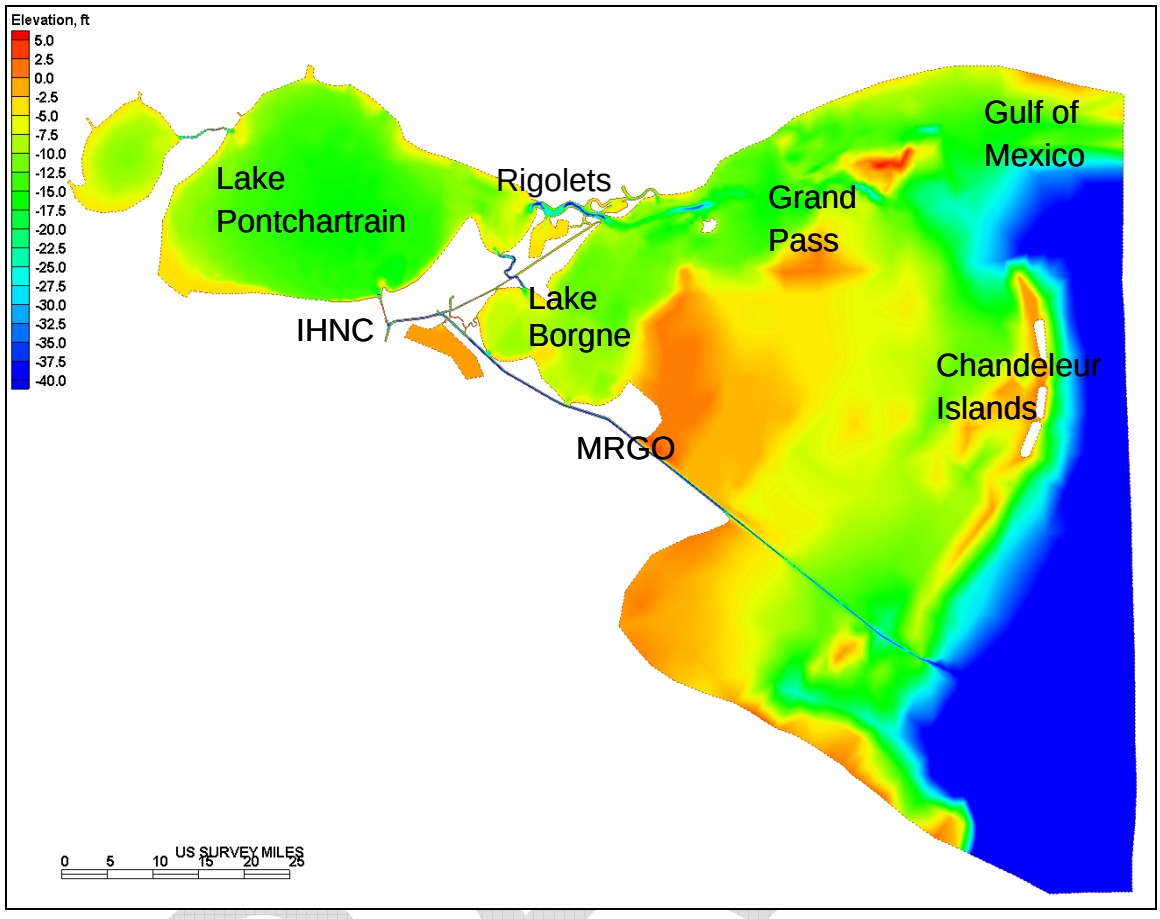

Figure 2-1. Model domain and bathymetry

Boundary Conditions

Boundary conditions for this model include river inflows, tidal water surface elevations, and wind forcings. This information is needed for August 2007 through October 2008 in order to perform the requested analyses.

The river inflows to the model domain are taken from the U.S. Geologic Survey streamflow database. Daily average values are applied to the model at six locations: the Pearl River, the Amite River, the Blind River, the Tchefuncte River, the Tickfaw River, and the Tangipahoa River. The locations of these rivers are shown in Figure 2-2. Flow from the Mississippi River into the Gulf of Mexico is accounted for in the tidal boundary condition since it does not enter directly into the model domain. Ungaged flows are not factored into the model, which includes any flow through the wetland areas along the Mississippi River.

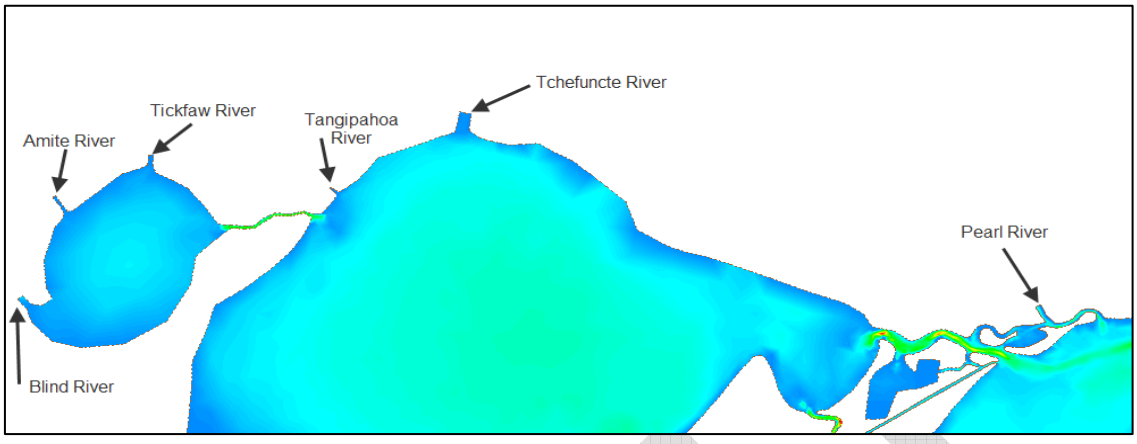

Figure 2-2. Location of river inflows

The tidal forcings for the hydrodynamic model are generated using 2008 NOAA gage data from Gulfport Harbor (gage #8745557) and Pilots Station East, SW Pass (gage #8760922). The harmonic constituents and the non-predicted signal for each station are used to generate a tidal forcing or water surface elevation at each node along the tidal boundary over the time of the simulation. The values for each node are determined by performing a linear interpolation of the amplitude and phase for each tidal constituent as well as for the nonpredicted signal. The tide is then reconstituted at each location along the boundary using these interpolated parameters. Again, details of this process and more information of the tidal boundary condition is available in Tate et al. 2009.

The wind data used were obtained from the Joint Air Force and Army Weather Information Network and the Air Force Combat Climatology Center in Ashville, NC. These data are hourly surface winds at the New Orleans International Airport (Station 722310 – KMSY). The wind signal is interpolated using a polynomial interpolation for the wind signal components to fill any data gaps.

DRAFT

3 Construction Sequence Plans

Model Scenarios

Two construction plan simulations are modeled in addition to the previous modeling efforts described in Tate et al. 2009. The two scenarios are modeled according to the analysis conditions requested by HPO in Tate et al. 2009 and the hydrodynamic results are provided to HPO. These results will be compared to an existing condition in which all waterways are open (Base), a plan condition in which the MRGO is closed at La Loutre (Plan 1), and a plan in which the MRGO is closed at La Loutre and south of Bayou Bienvenue and gate structures exist on the Bayou Bienvenue and GIWW (Plan 2). These conditions are labeled to correspond to the same conditions in the previous research and reports and details of these plans are given in the list below.

- Base - fully open MRGO, GIWW, and IHNC (Figure 3-1)
- Plan 1 – close the MRGO at La Loutre (Figure 3-2)
- Plan 2 – close the MRGO at La Loutre, include the Borgne alignment (close the MRGO south of Bayou Bienvenue, 56 ft X 8 ft gate on Bayou Bienvenue, and two 150 ft X 16 ft gates on GIWW) (Figure 3-3)

The two construction sequences are intended to show how the actual construction process may affect the flows and water surface elevations in the surrounding areas of the system. While constructing these hurricane protection structures, cofferdams will be in place at various times, restricting the amount of flow passing certain locations, at times completely cutting off the channel. These cofferdams will be labeled as a closed pathway in the following figures. The construction sequence conditions are given below.

- February 2010 – close the MRGO at La Loutre, close the MRGO south of Bayou Bienvenue, cofferdam at the 56 ft X 8 ft gate on Bayou Bienvenue, cofferdam at the 150 ft X 16 ft sector gate on

DRAFT

GIWW, open the 150 ft X 16 ft barge gate on GIWW, Seabrook area unchanged from Base (Figure 3-4)

- March 2010 - close the MRGO at La Loutre, close the MRGO south of Bayou Bienvenue, cofferdam at the 56 ft X 8 ft gate on Bayou Bienvenue, cofferdam at the 150 ft X 16 ft sector gate on GIWW, open the 150 ft X 16 ft barge gate on GIWW, Seabrook opening completely closed off for flow with cofferdam (Figure 3-5)

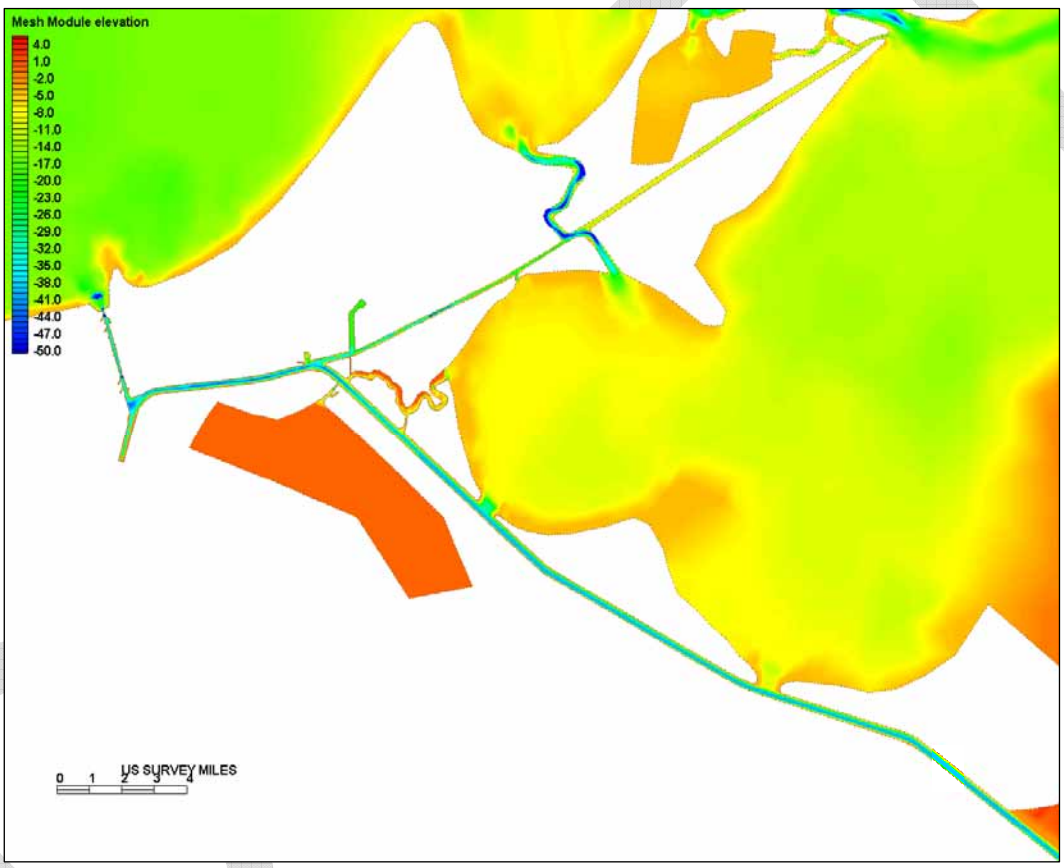

Figure 3-1. Base configuration: no closures, no structures

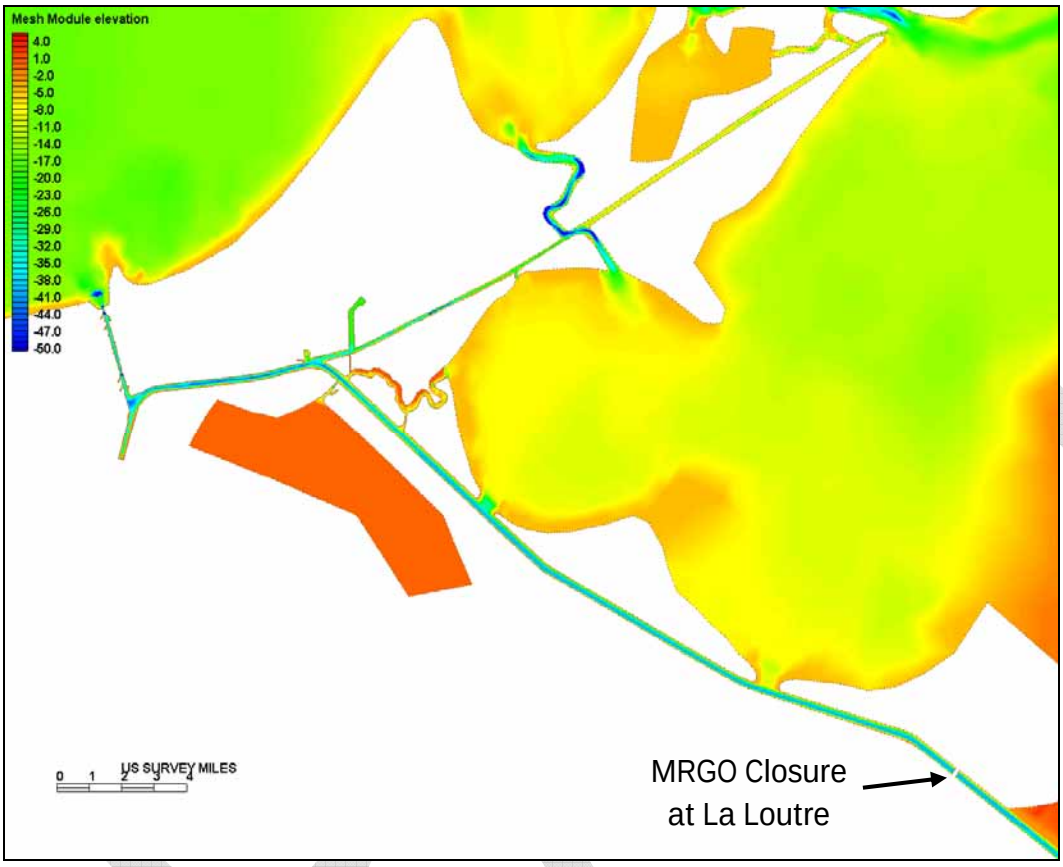

Figure 3-2. Plan 1 configuration: close the MRGO at La Loutre

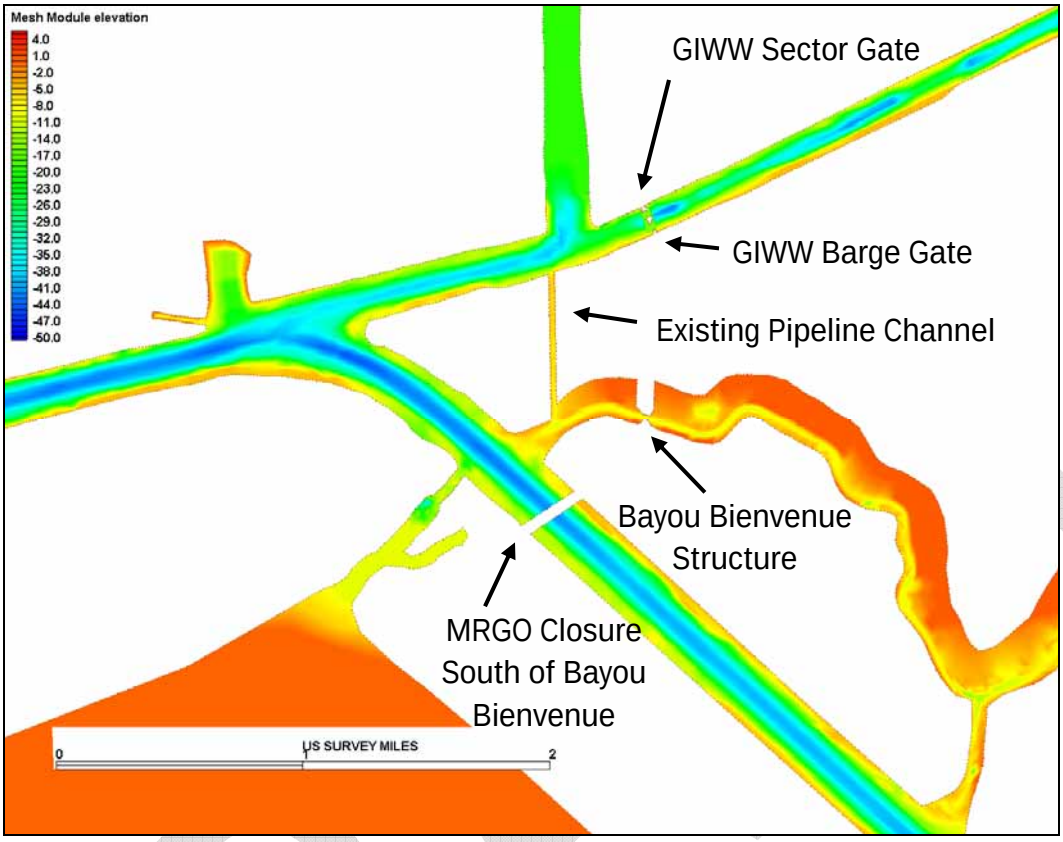

Figure 3-3. Plan 2 configuration: includes Plan 1 and the Borgne alignment (56 ft X 8 ft gate on Bayou Bienvenue, and two 150 ft X 16 ft gates on GIWW)

DRAFT

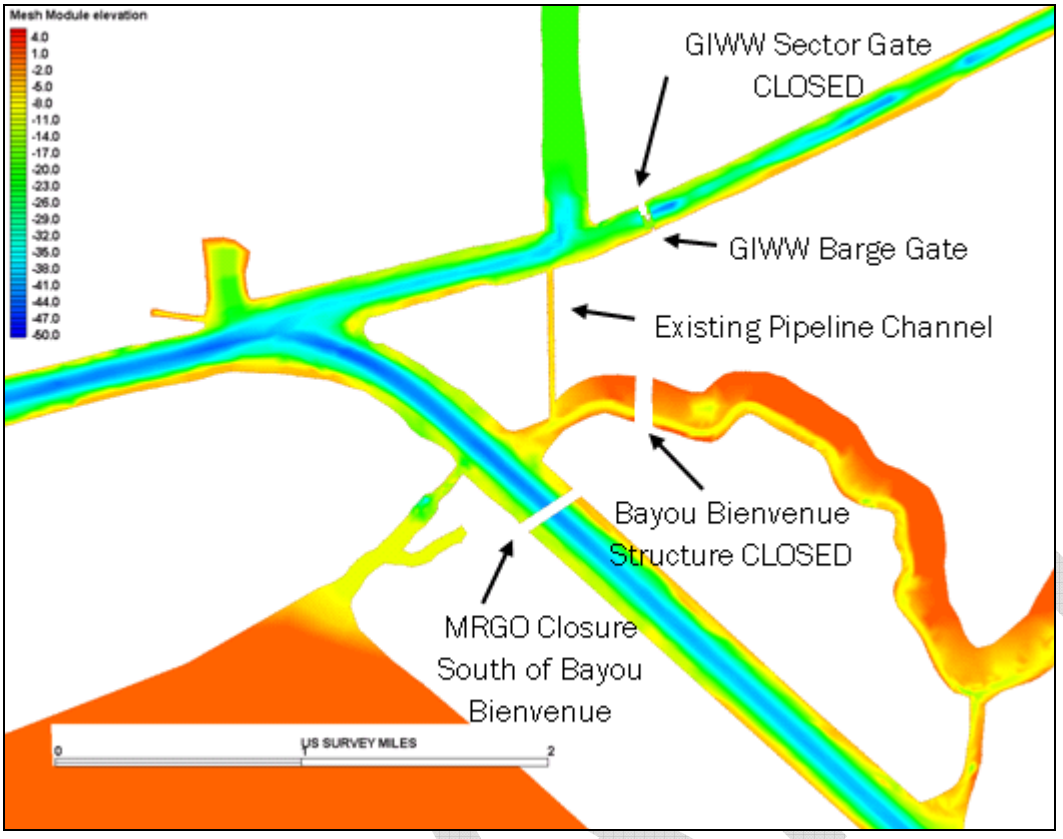

Figure 3-4. February 2010 configuration: close the MRGO at La Loutre, close the MRGO south of Bayou Bienvenue, cofferdam at the Bayou Bienvenue gate, cofferdam at the sector gate on GIWW, and open the 150 ft X 16 ft barge gate on GIWW

DRAFT

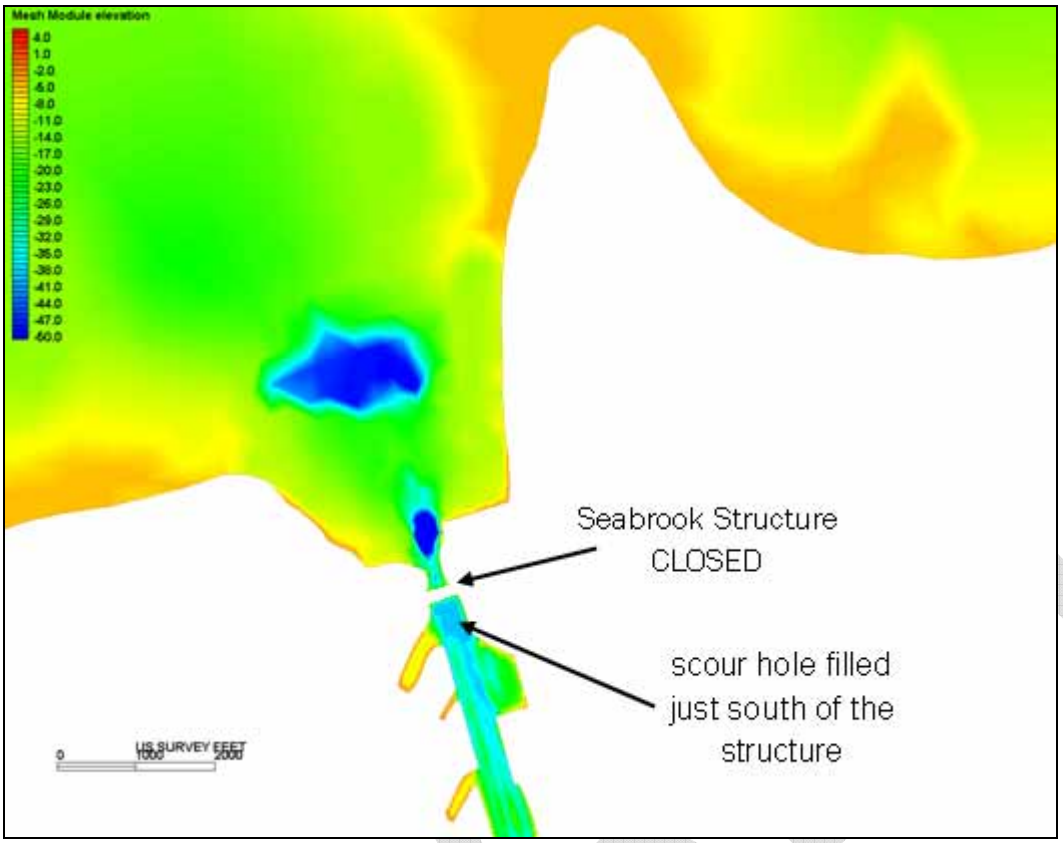

Figure 3-5. March 2010 configuration: includes February 2010 configuration with a cofferdam at the Seabrook structure as well

The hydrodynamic simulations for all conditions are run for two different time periods. The analysis period was 4 weeks. A two week spin-up period is included in the hydrodynamic simulations prior to the analysis period. The two time periods used for this study are August 15 – September 15, 2007 (labeled as September) and March 1 – 31, 2008. A general picture of the tidal signal near the Gulf boundary for these two time periods is shown in Figures 3-6 and 3-7. The wind speeds at the New Orleans International Airport for these periods are given in Figures 3-8 and 3-9. It is apparent in these figures that the March winds and tide are indicative of the spring season when conditions are more erratic due to front passages and rain events. The September period shows lower wind speeds and a more typical diurnal tide signal which is expected in the Gulf of Mexico.

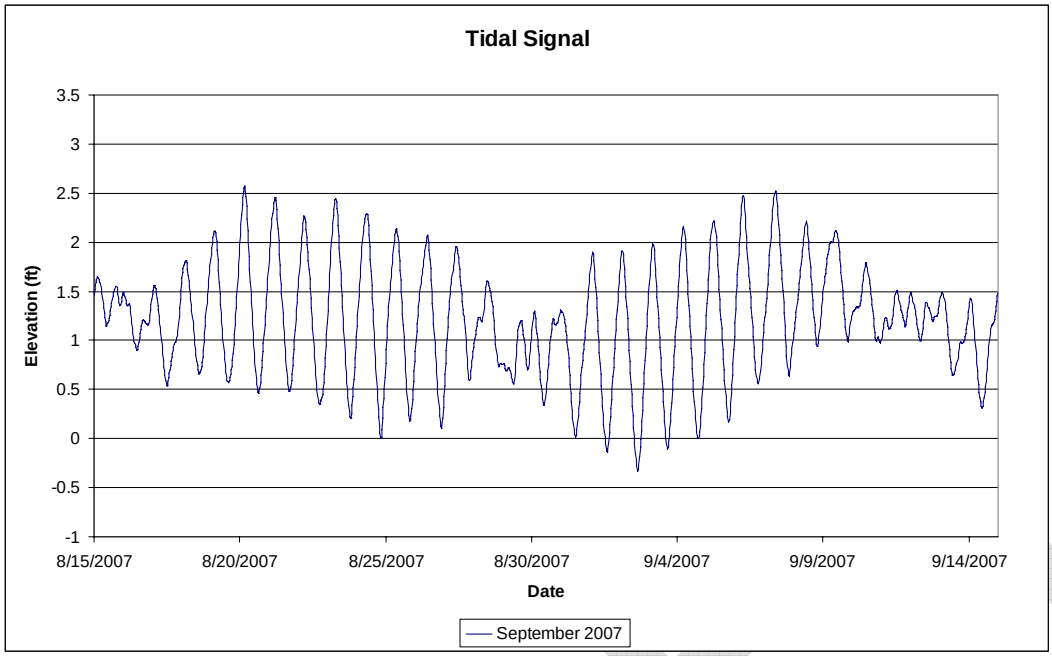

Figure 3-6. Tide signal for the September analysis period

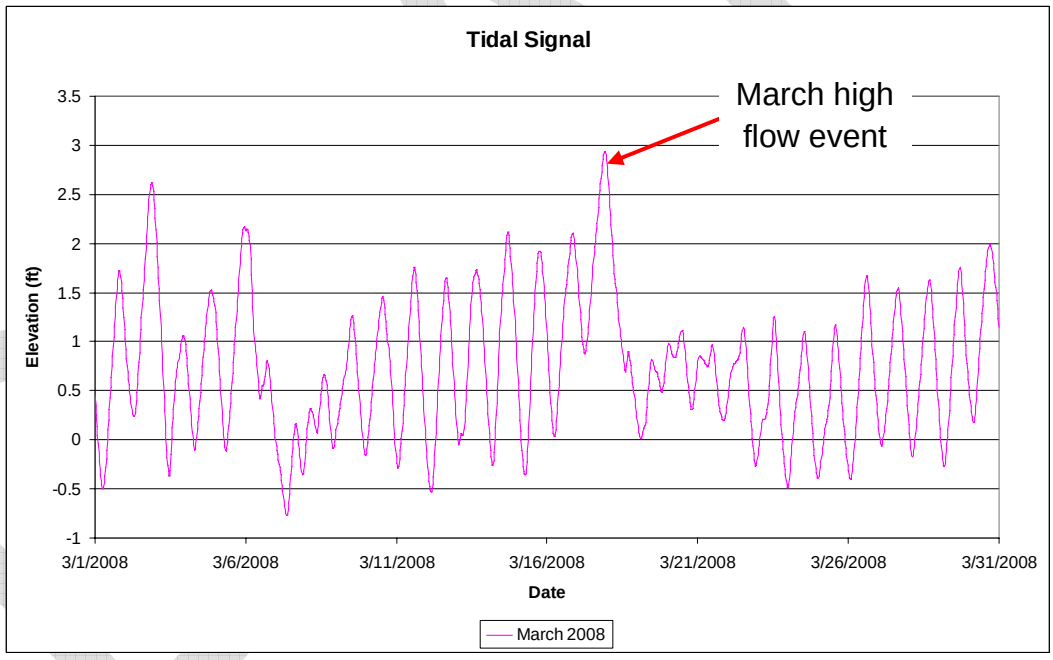

Figure 3-7. Tide signal for the March analysis period

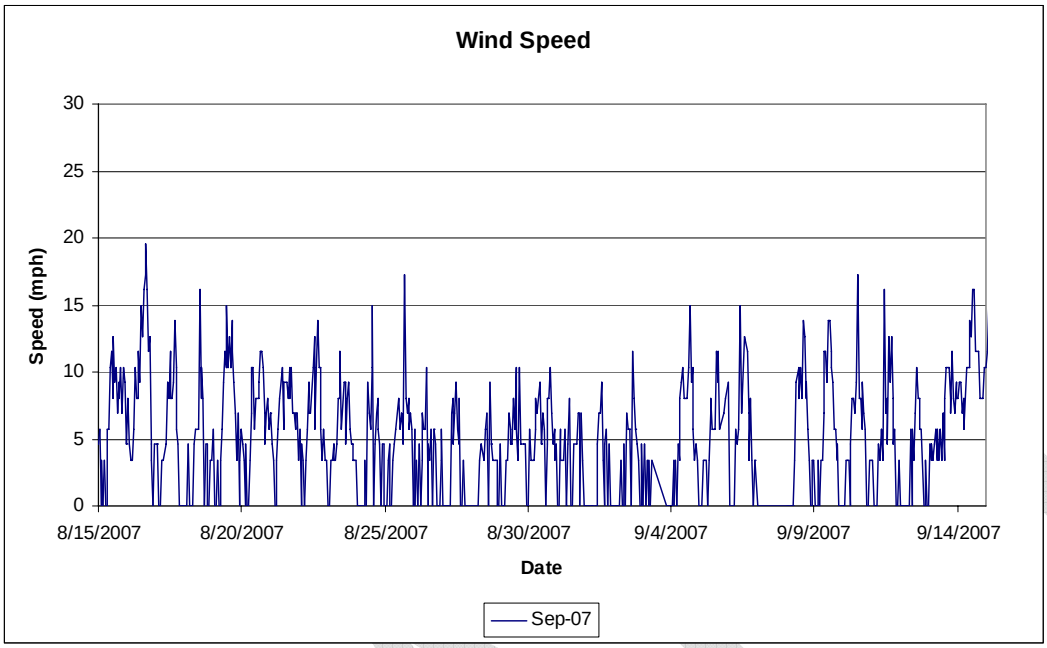

Figure 3-8. Wind signal for the September analysis period

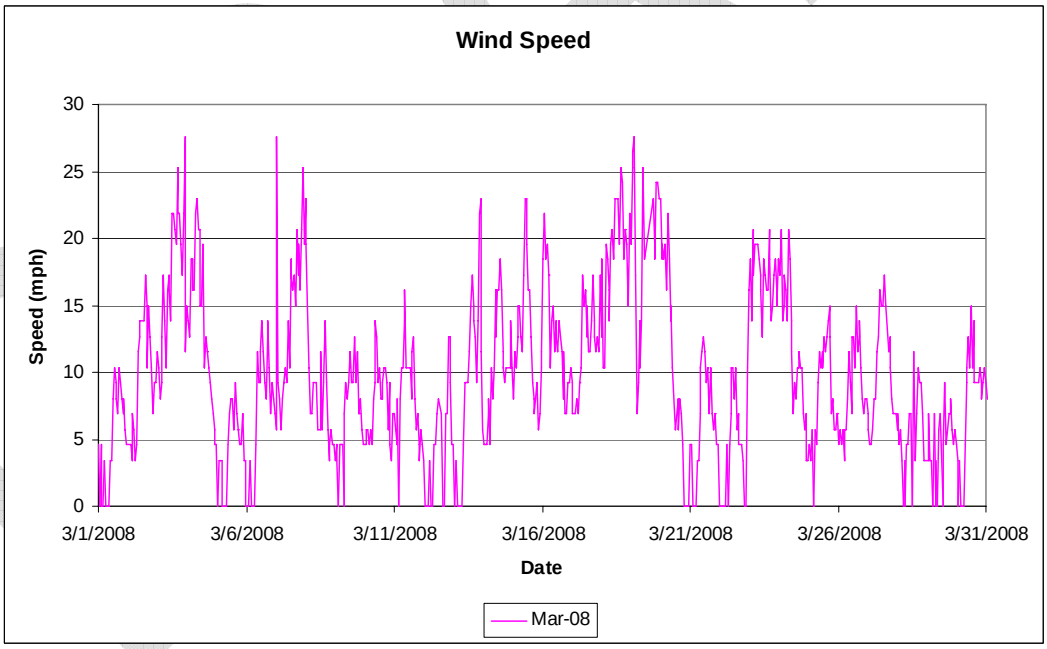

Figure 3-9. Wind signal for the March analysis period

4 Hydrodynamic Results

The results of the hydrodynamic simulations are presented here. An analysis of how the plan conditions affect the velocities and water surface elevations in the area of the structures is given in this section.

Velocity Magnitudes

Velocity data are taken in the location of the structures for the GIWW barge gate and the Seabrook structure. Data is not taken in the Bayou Bienvenue structure or at the GIWW sector gate since there is a cofferdam in place at these locations. Since there is also a cofferdam at the Seabrook structure in the March 2010 condition, no data is presented for that situation. Data is also compared at locations in Chef Menteur and the Rigolets. Figures 4-1 through 4-3 show the locations of velocity data comparisons. For the Base, Plan 1, and Plan 2 comparison conditions, data are analyzed at a location north of the Seabrook structure location where the velocities are greatest.

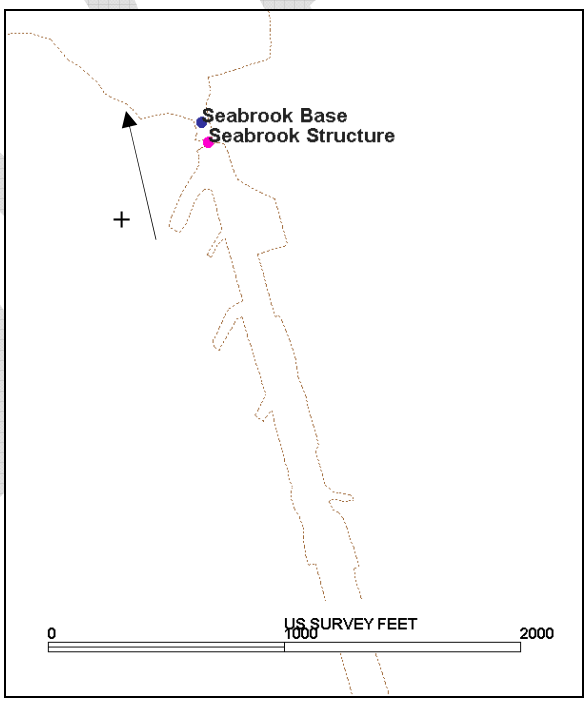

Figure 4-1. Hydrodynamic analysis locations - Seabrook

DRAFT

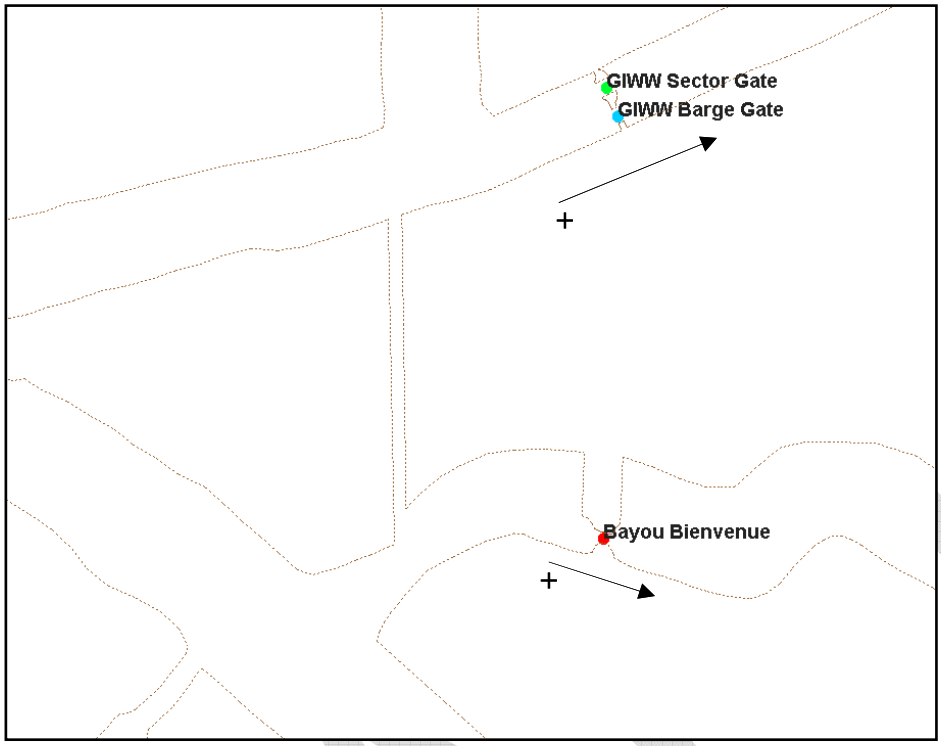

Figure 4-2. Hydrodynamic analysis locations – Bayou Bienvenue Structure, GIWW Sector Gate, and GIWW Barge Gate

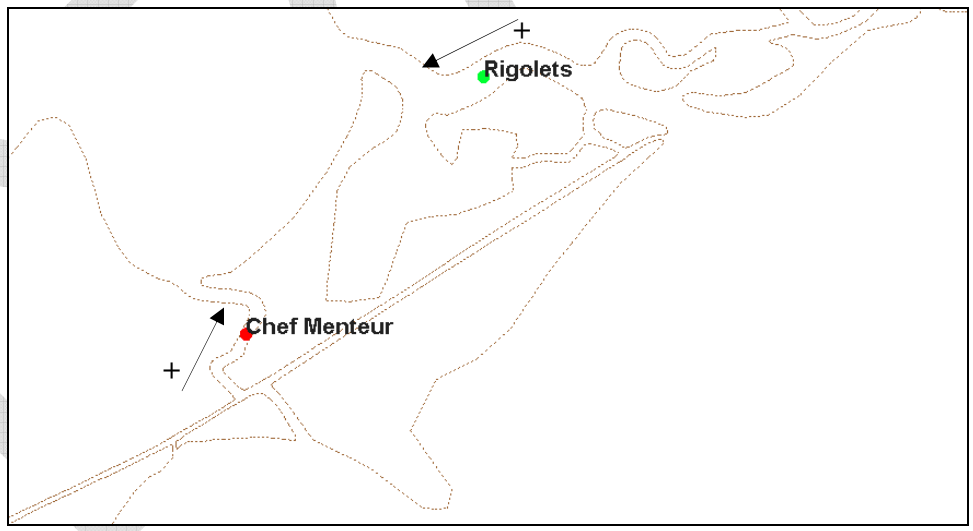

Figure 4-3. Hydrodynamic analysis locations – Chef Menteur and Rigolets

The average velocity for flood and ebb are determined at each location and time period for all simulation conditions as are the maximum velocities for all conditions. Since there is a circulation within this system through the GIWW, the definition of flood and ebb can be misleading. For this reason a definition of positive and negative or flood and ebb is necessary. Positive values are defined as those directed predominantly toward the north or east and negative values are defined as those directed predominantly toward the south or west, except at the Chef Menteur and Rigolets where positive flow is into Lake Pontchartrain and negative flow is toward the GIWW or Lake Borgne. The arrows in Figures 4-1 through 4-3 show the positive direction for each location. The results of this analysis are given in Figures 4-4 through 4-11. A direction arrow is included for each location to help define the flow direction.

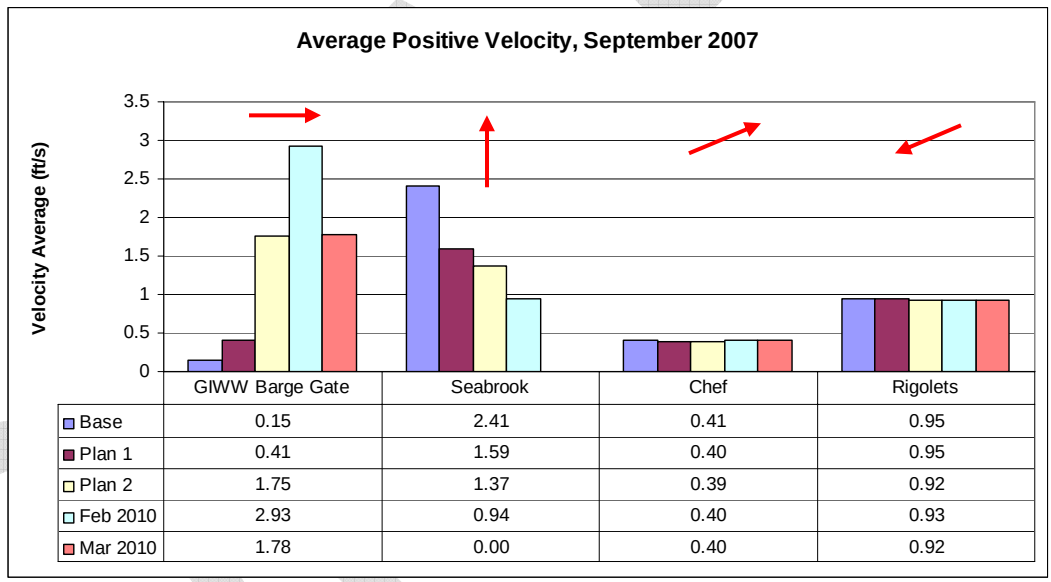

	GIWW Barge Gate	Seabrook	Chef	Rigolets
Base	0.15	2.41	0.41	0.95
Plan 1	0.41	1.59	0.40	0.95
Plan 2	1.75	1.37	0.39	0.92
Feb 2010	2.93	0.94	0.40	0.93
Mar 2010	1.78	0.00	0.40	0.92

Figure 4-4. Velocity average for September (positive)

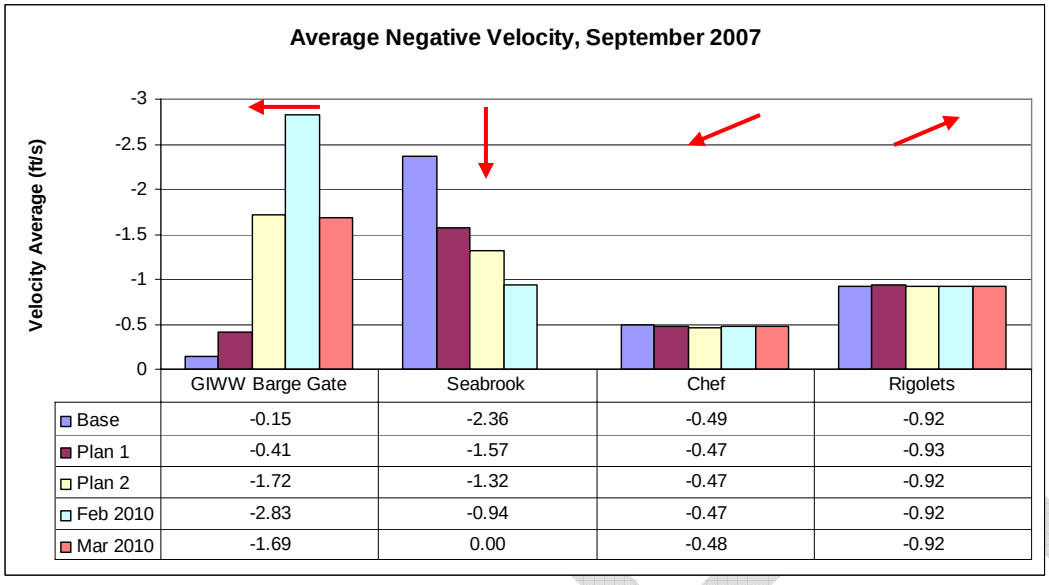

	GIWW Barge Gate	Seabrook	Chef	Rigolets
Base	-0.15	-2.36	-0.49	-0.92
Plan 1	-0.41	-1.57	-0.47	-0.93
Plan 2	-1.72	-1.32	-0.47	-0.92
Feb 2010	-2.83	-0.94	-0.47	-0.92
Mar 2010	-1.69	0.00	-0.48	-0.92

Figure 4-5. Velocity average for September (negative)

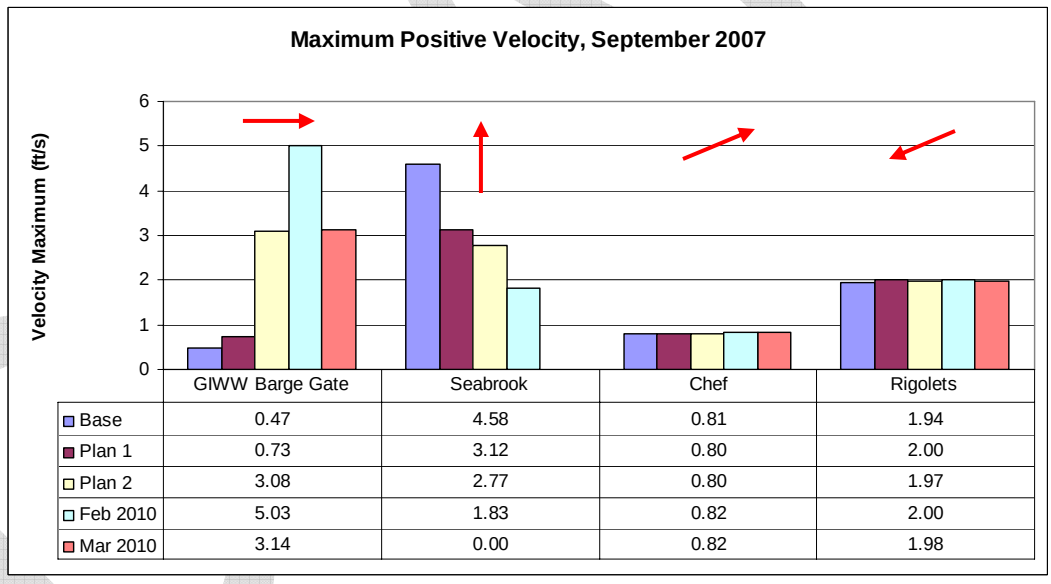

	GIWW Barge Gate	Seabrook	Chef	Rigolets
Base	0.47	4.58	0.81	1.94
Plan 1	0.73	3.12	0.80	2.00
Plan 2	3.08	2.77	0.80	1.97
Feb 2010	5.03	1.83	0.82	2.00
Mar 2010	3.14	0.00	0.82	1.98

Figure 4-6. Velocity maximum for September (positive)

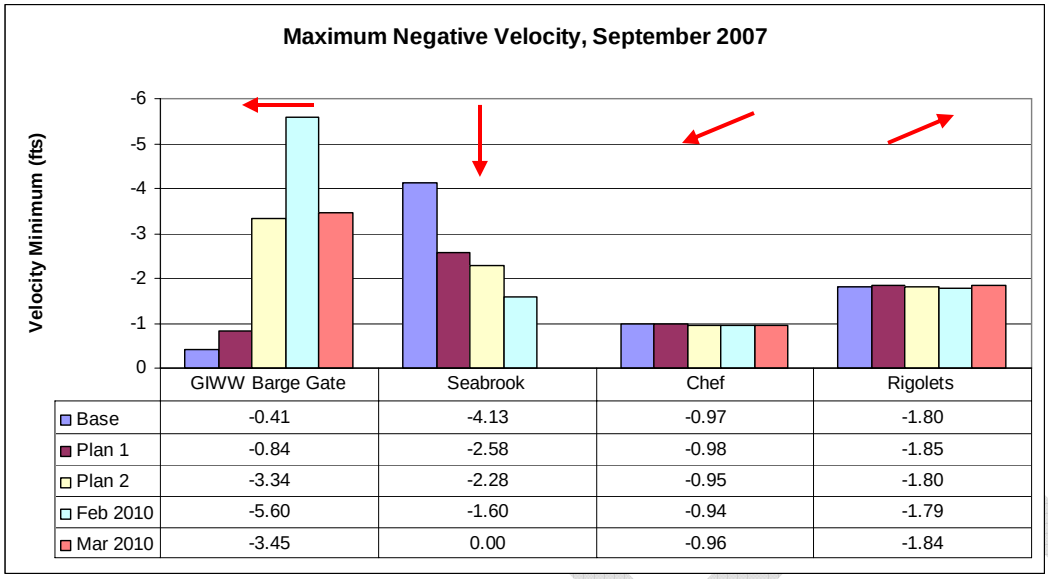

	GIWW Barge Gate	Seabrook	Chef	Rigolets
Base	-0.41	-4.13	-0.97	-1.80
Plan 1	-0.84	-2.58	-0.98	-1.85
Plan 2	-3.34	-2.28	-0.95	-1.80
Feb 2010	-5.60	-1.60	-0.94	-1.79
Mar 2010	-3.45	0.00	-0.96	-1.84

Figure 4-7. Velocity minimum for September (negative)

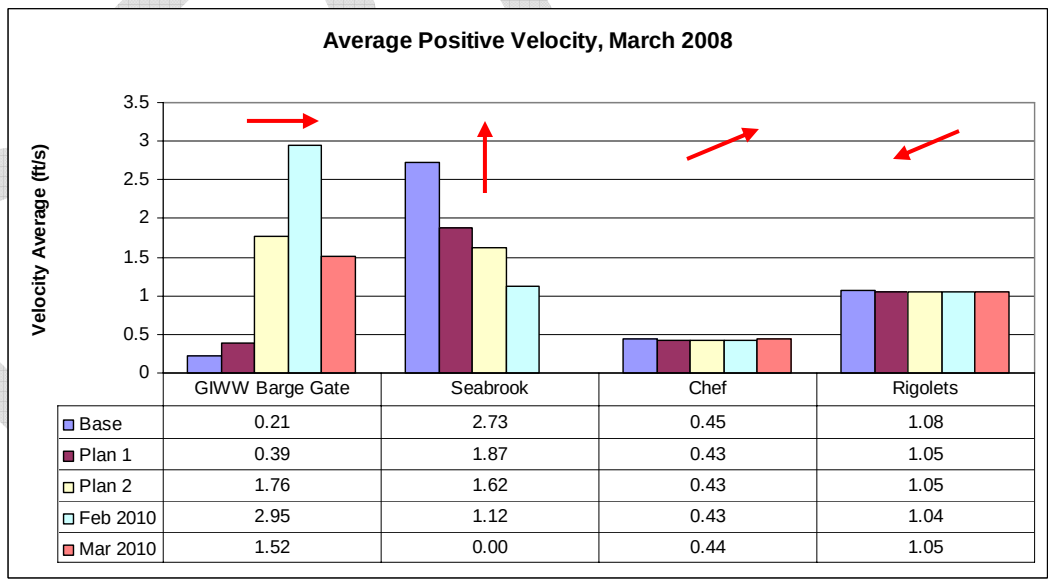

	GIWW Barge Gate	Seabrook	Chef	Rigolets
Base	0.21	2.73	0.45	1.08
Plan 1	0.39	1.87	0.43	1.05
Plan 2	1.76	1.62	0.43	1.05
Feb 2010	2.95	1.12	0.43	1.04
Mar 2010	1.52	0.00	0.44	1.05

Figure 4-8. Velocity average for March (positive)

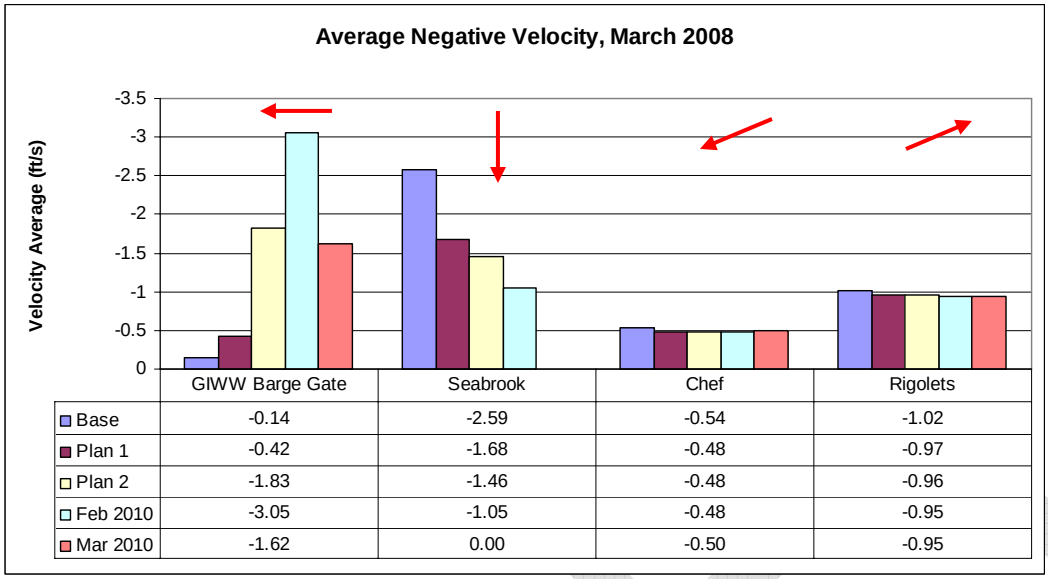

	GIWW Barge Gate	Seabrook	Chef	Rigolets
Base	-0.14	-2.59	-0.54	-1.02
Plan 1	-0.42	-1.68	-0.48	-0.97
Plan 2	-1.83	-1.46	-0.48	-0.96
Feb 2010	-3.05	-1.05	-0.48	-0.95
Mar 2010	-1.62	0.00	-0.50	-0.95

Figure 4-9. Velocity average for March (negative)

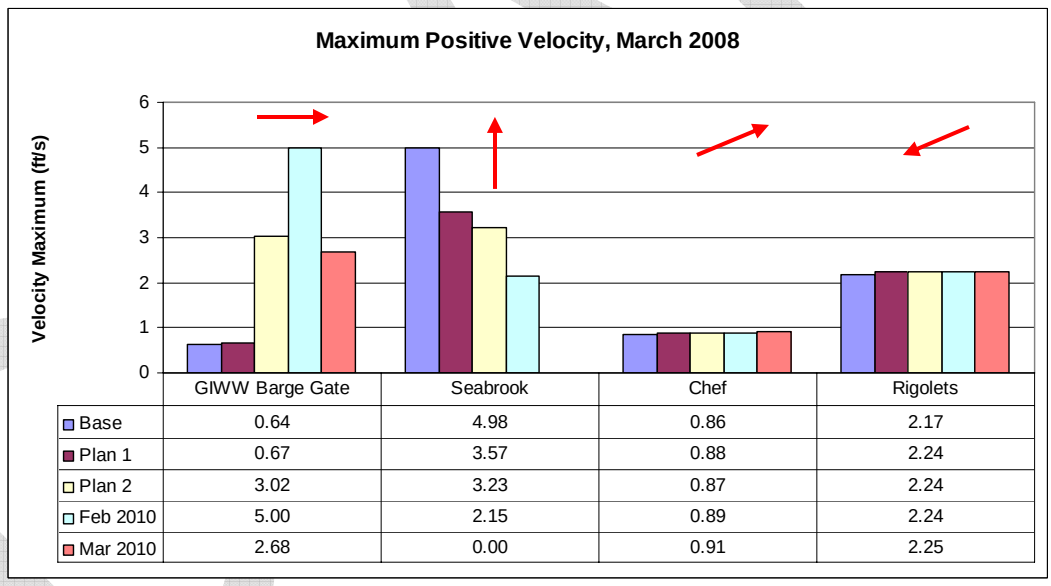

	GIWW Barge Gate	Seabrook	Chef	Rigolets
Base	0.64	4.98	0.86	2.17
Plan 1	0.67	3.57	0.88	2.24
Plan 2	3.02	3.23	0.87	2.24
Feb 2010	5.00	2.15	0.89	2.24
Mar 2010	2.68	0.00	0.91	2.25

Figure 4-10. Velocity maximum for March (positive)

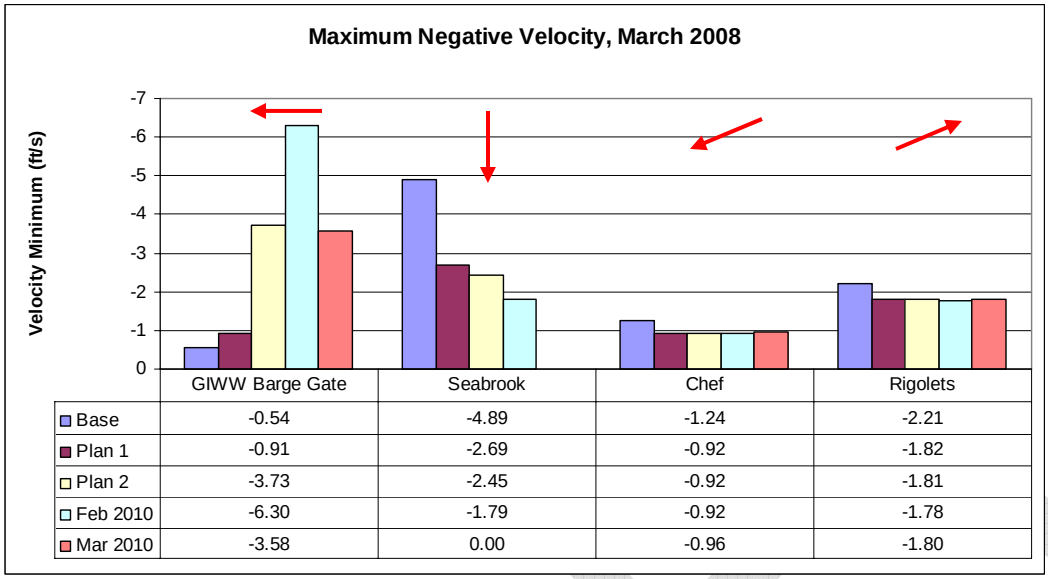

Figure 4-11. Velocity minimum for March (negative)

The February 2010 gate closure sequence included cofferdams at the GIWW sector gate and the Bayou Bienvenue gate (completely closing the waterway) along with both MRGO closures. This means that flow through the GIWW must pass through the 150 ft wide barge gate. By forcing all of the flow through this structure, the velocity increases greatly as noted in the previous figures for both September and March. However, the velocities at Seabrook are reduced because the smaller width on the GIWW limits the amount of exchange at Seabrook. By making velocity comparisons at Chef Menteur and Rigolets, it can be determined how wide the effects of the construction is felt. Based on the model results, the effects are limited to the area of the structures since there is very little change at Chef Menteur and Rigolets.

The March 2010 construction plan adds a cofferdam at Seabrook. By shutting off this entrance to Lake Pontchartrain, the overall water exchange between Lake Borgne and Lake Pontchartrain through the GIWW is reduced, as supported by the reduction in velocity at the GIWW barge gate. Again, the effects do not extend too far into the system since there are no significant changes in velocity at Chef Menteur and Rigolets.

The maximum velocity magnitudes, however, only occur during a small fraction of the simulation time. A percent exceedance (i.e. percent less than) analysis is performed to determine how often during the four week

simulation periods the velocity magnitudes are within certain ranges. Figures 4-13 through 4-24 show the percent less than plots for the locations given in Figure 4-11. As with the previous analysis, data is not taken in the Bayou Bienvenue structure or the GIWW sector gate since these locations are blocked of any flow. No data is given for the Seabrook structure in the March 2010 condition since a cofferdam is in place under this plan. These locations are the same as those in the previous velocity analysis (see Figures 4-1 and 4-2) as well as additional locations in Lake Borgne, Lake Pontchartrain, Chef Menteur, and the Rigolets. These plots show velocity magnitude on the x-axis and percentage of time on the y-axis. At the maximum velocity magnitude, the percentage is almost 100 since the velocity is equal to or less than this value over the length of the simulation. All lines cross zero at 0% since the velocity is always greater than zero. Where each line crosses 50% the velocity is greater half the time and less half the time over the 4 week analysis period.

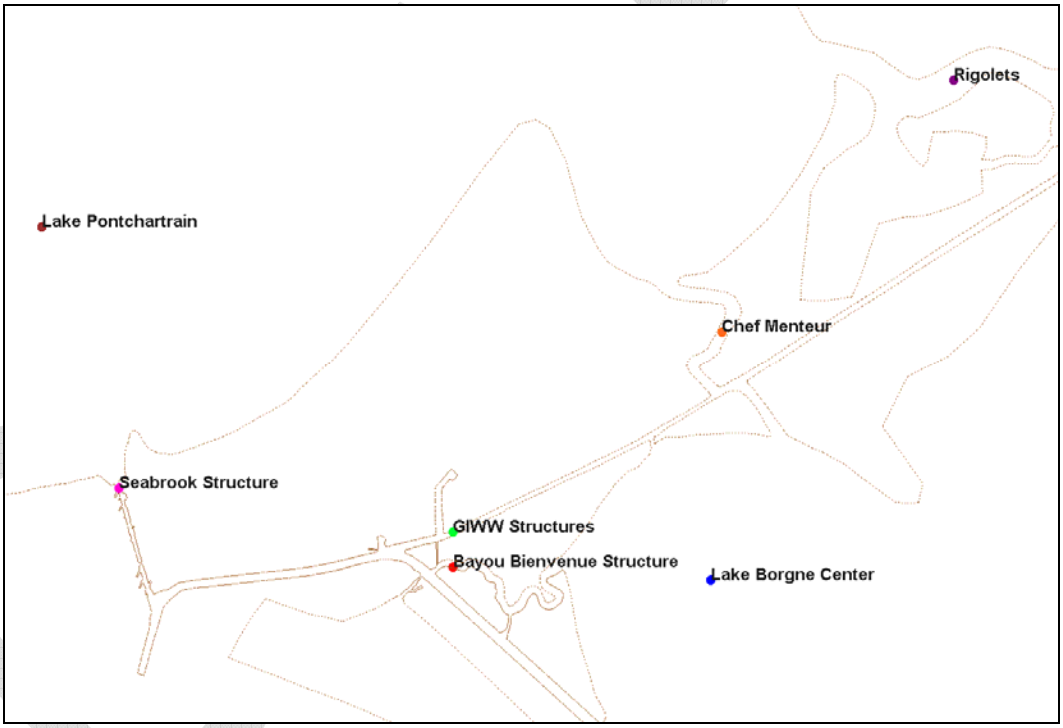

Figure 4-12. Percent exceedance of velocity magnitude analysis locations

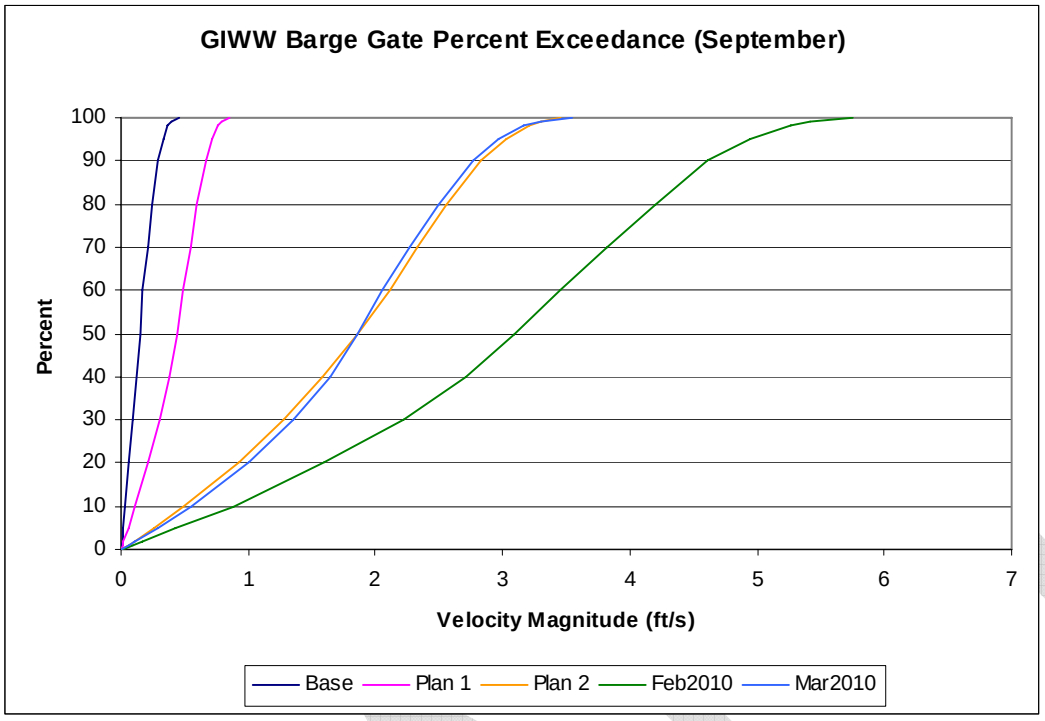

Figure 4-13. GIWW Barge Gate percent exceedance plot for September

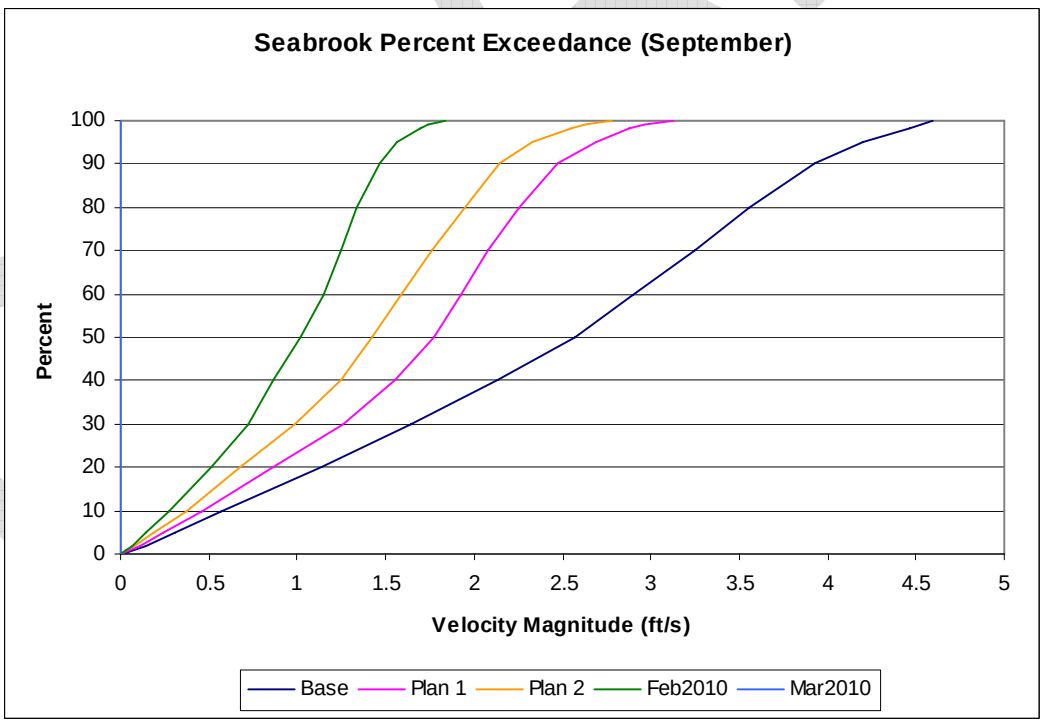

Figure 4-14. Seabrook percent exceedance plot for September

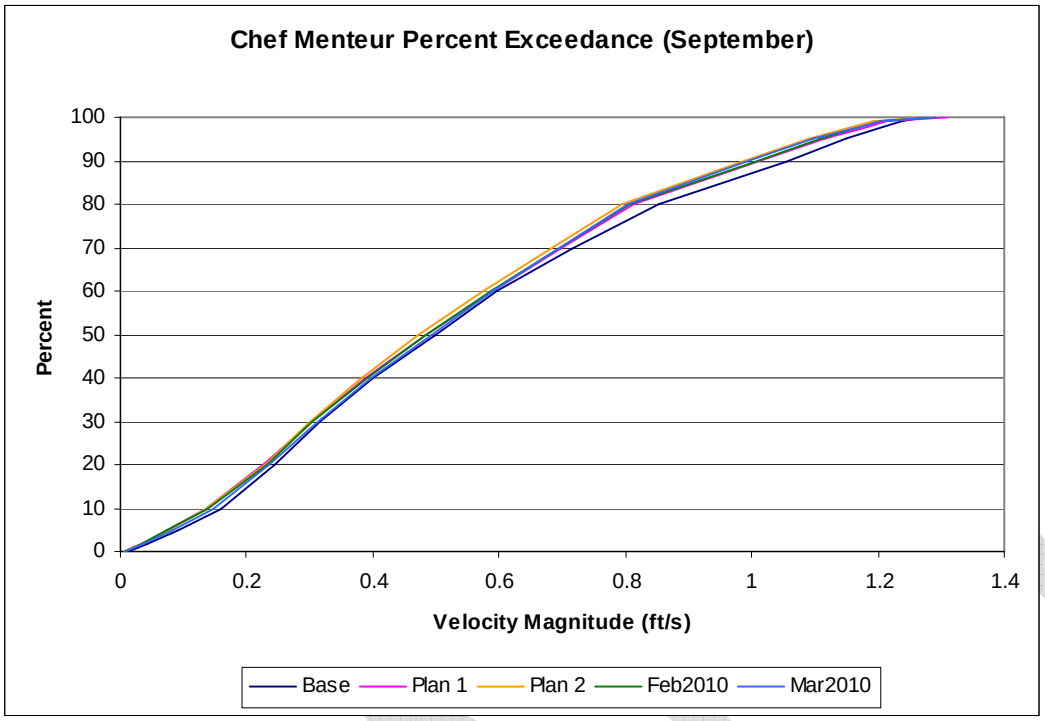

Figure 4-15. Chef Menteur percent exceedance plot for September

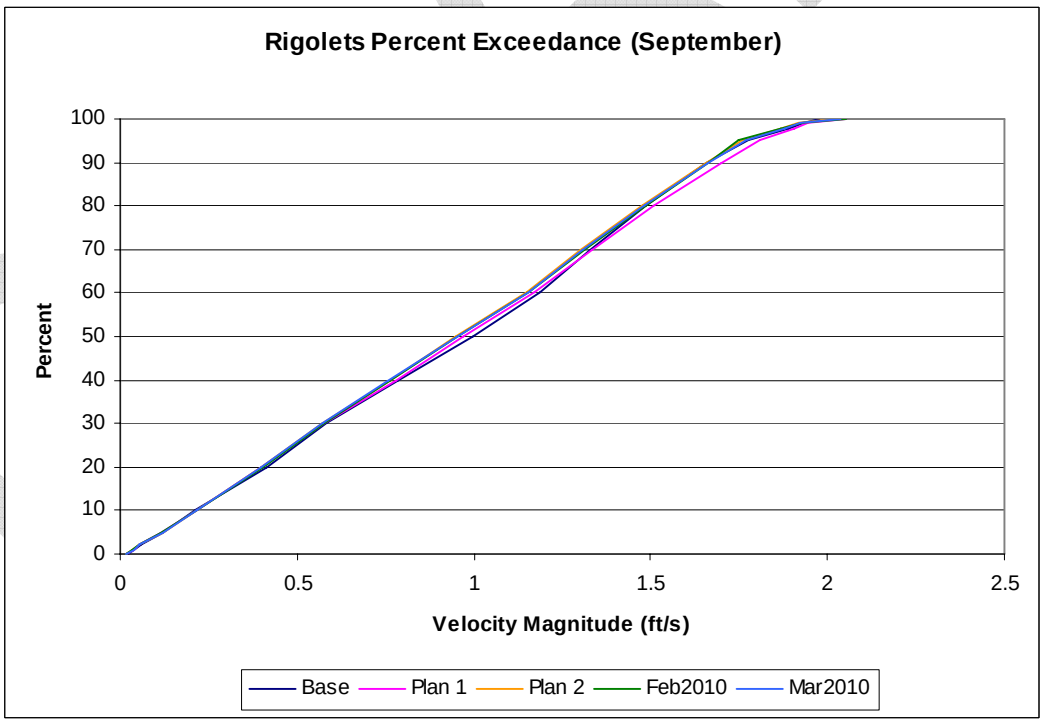

Figure 4-16. Rigolets percent exceedance plot for September

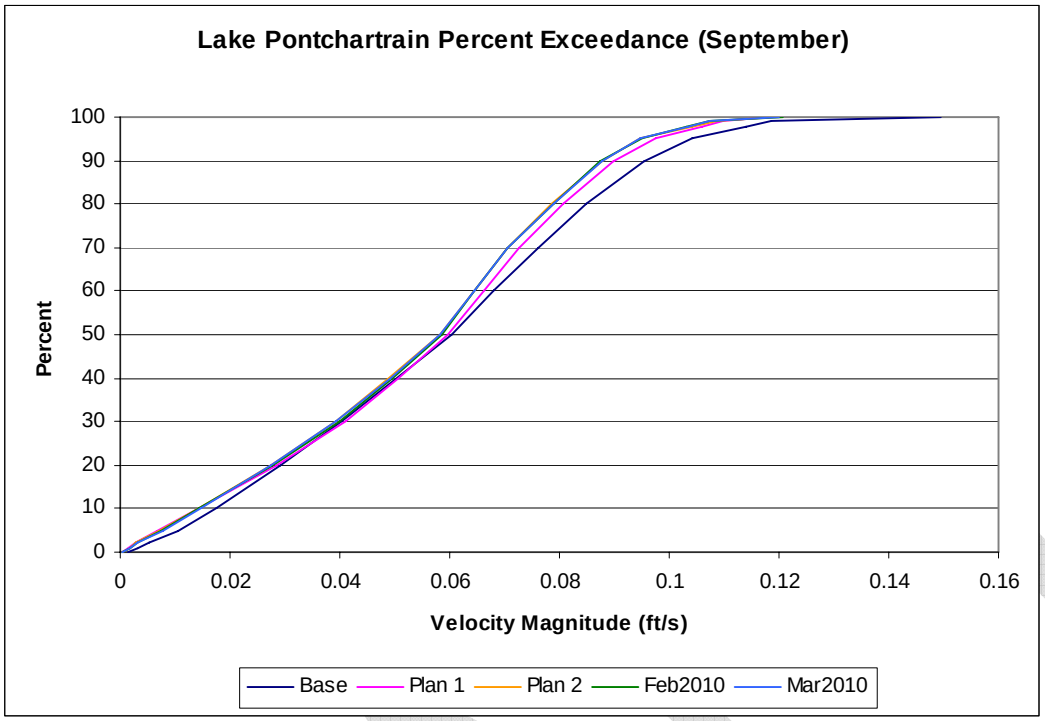

Figure 4-17. Lake Pontchartrain percent exceedance plot for September

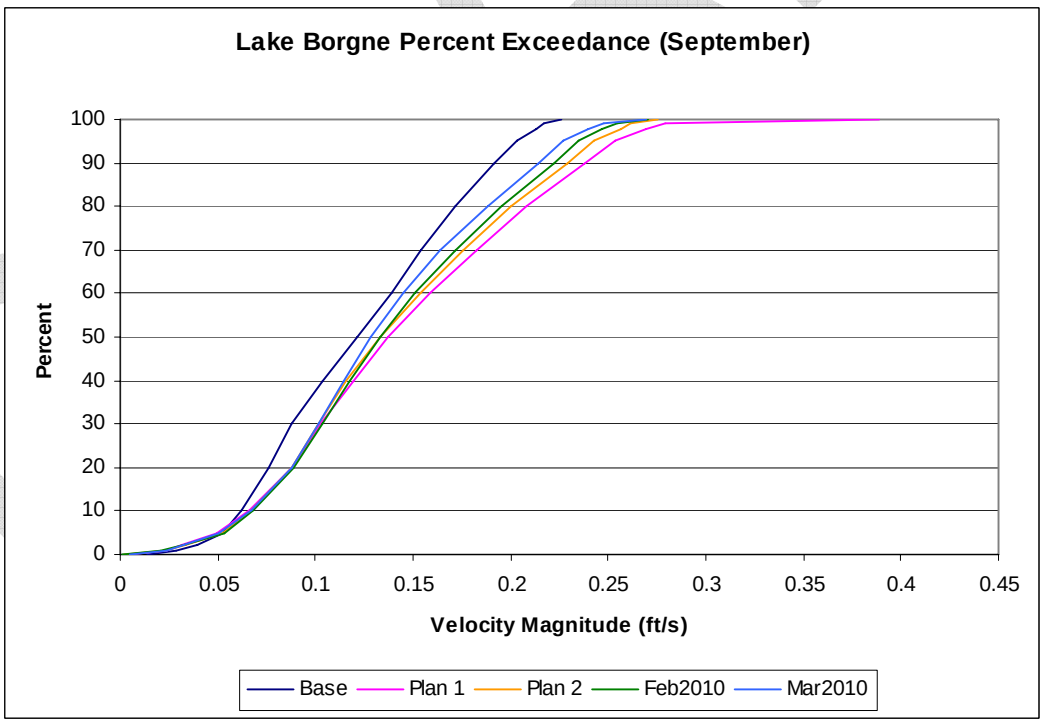

Figure 4-18. Lake Borgne percent exceedance plot for September

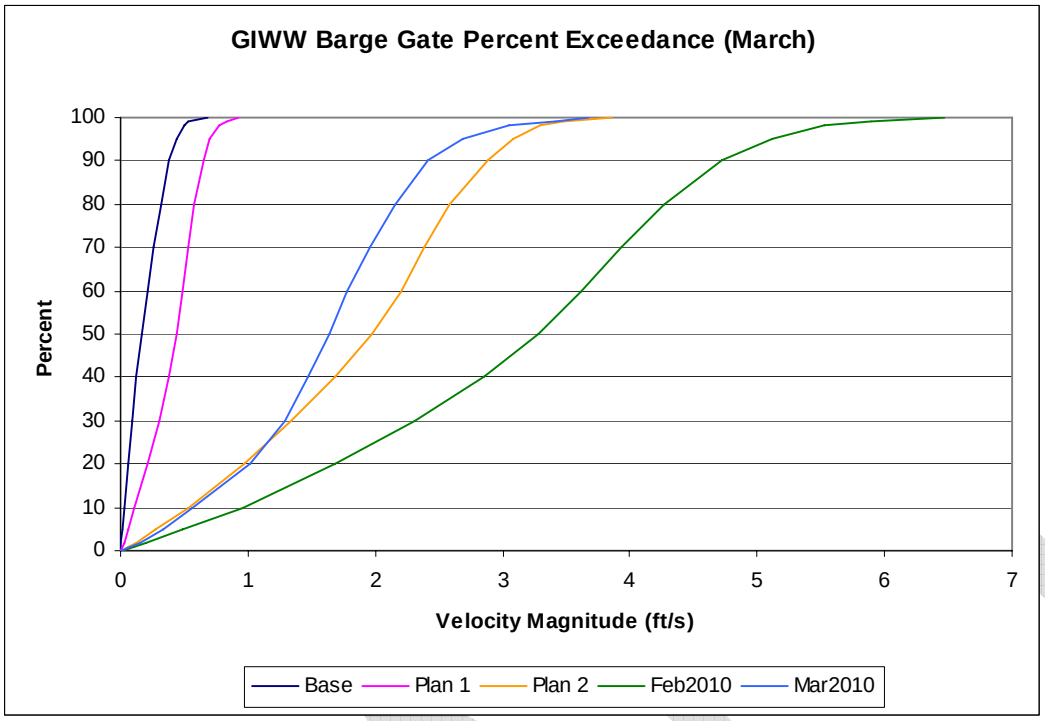

Figure 4-19. GIWW Barge Gate percent exceedance plot for March

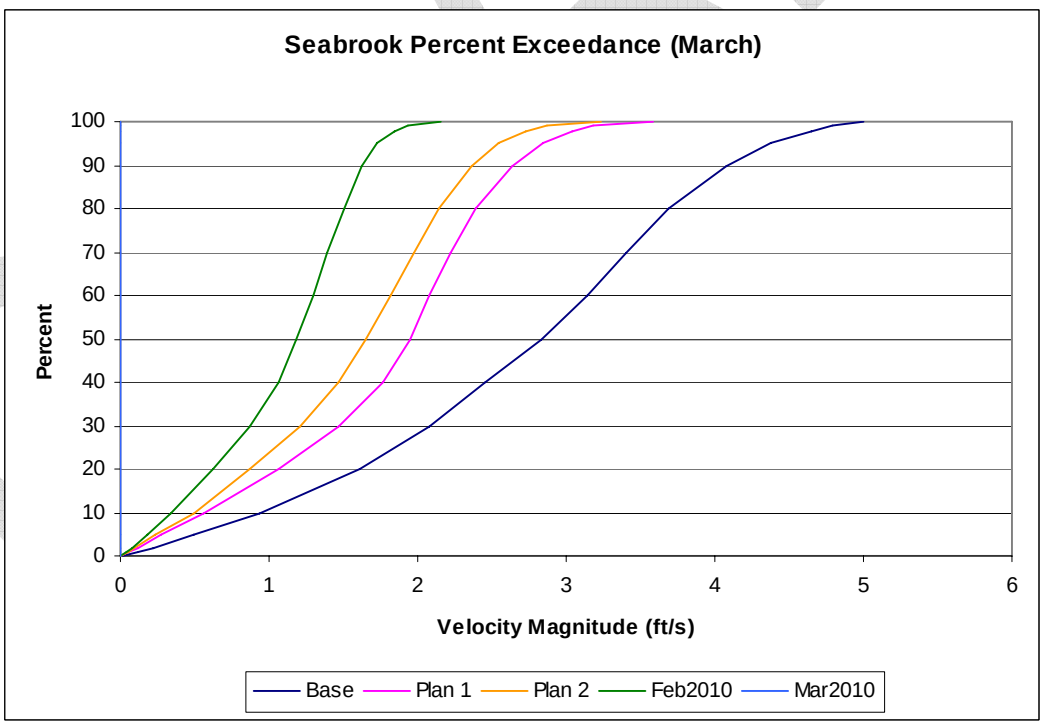

Figure 4-20. Seabrook percent exceedance plot for March

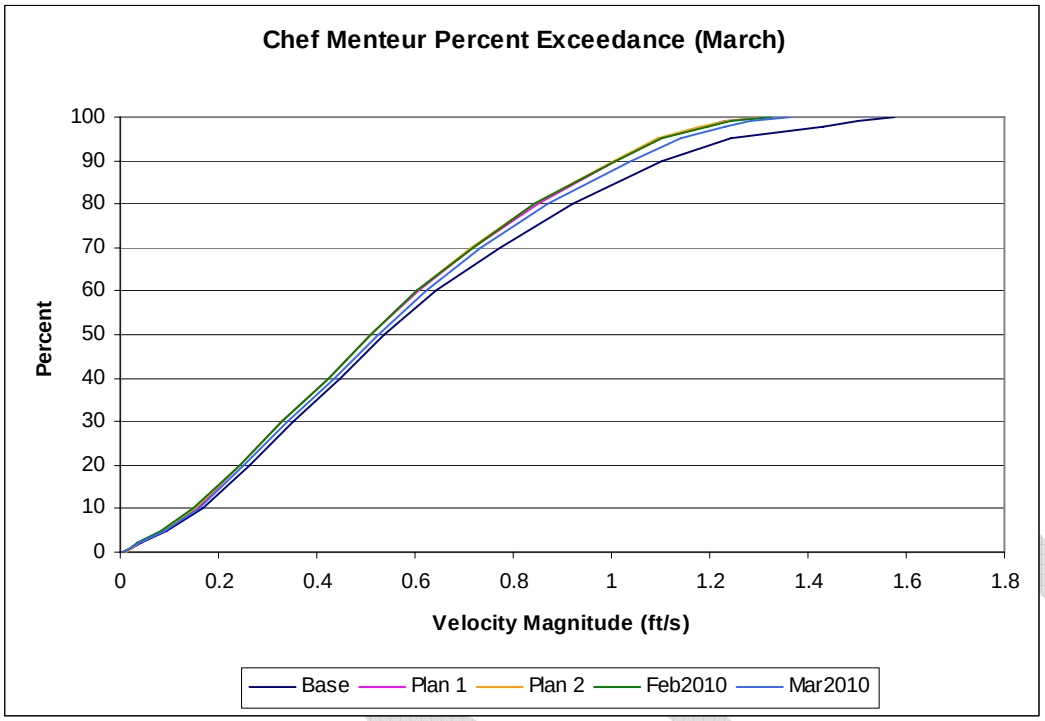

Figure 4-21. Chef Menteur percent exceedance plot for March

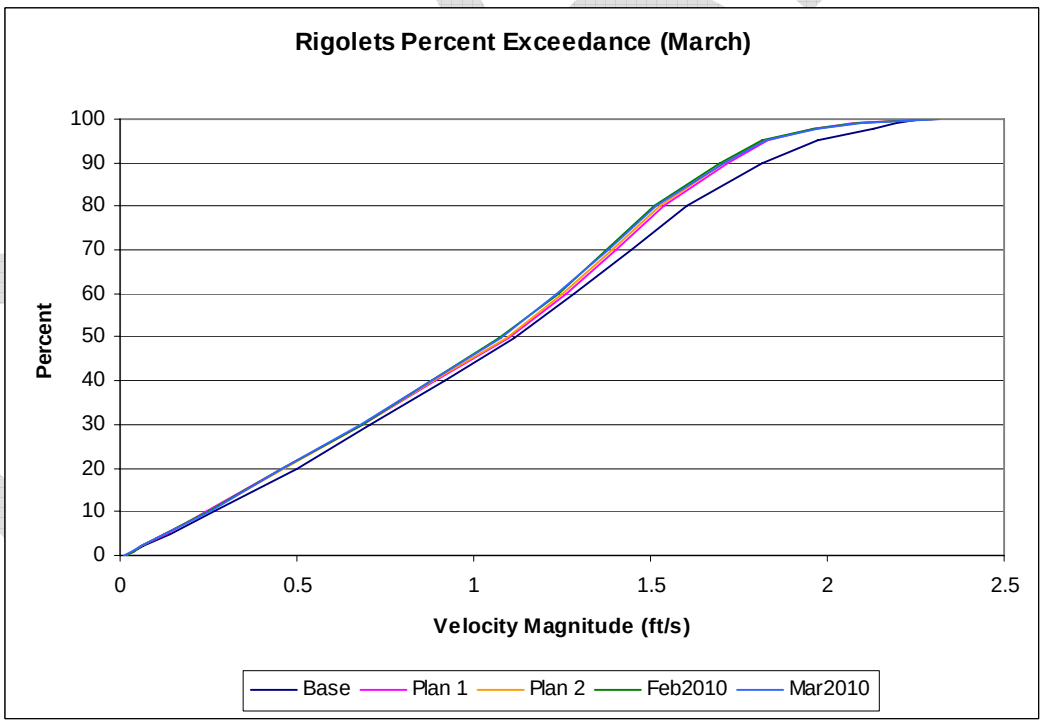

Figure 4-22. Rigolets percent exceedance plot for March

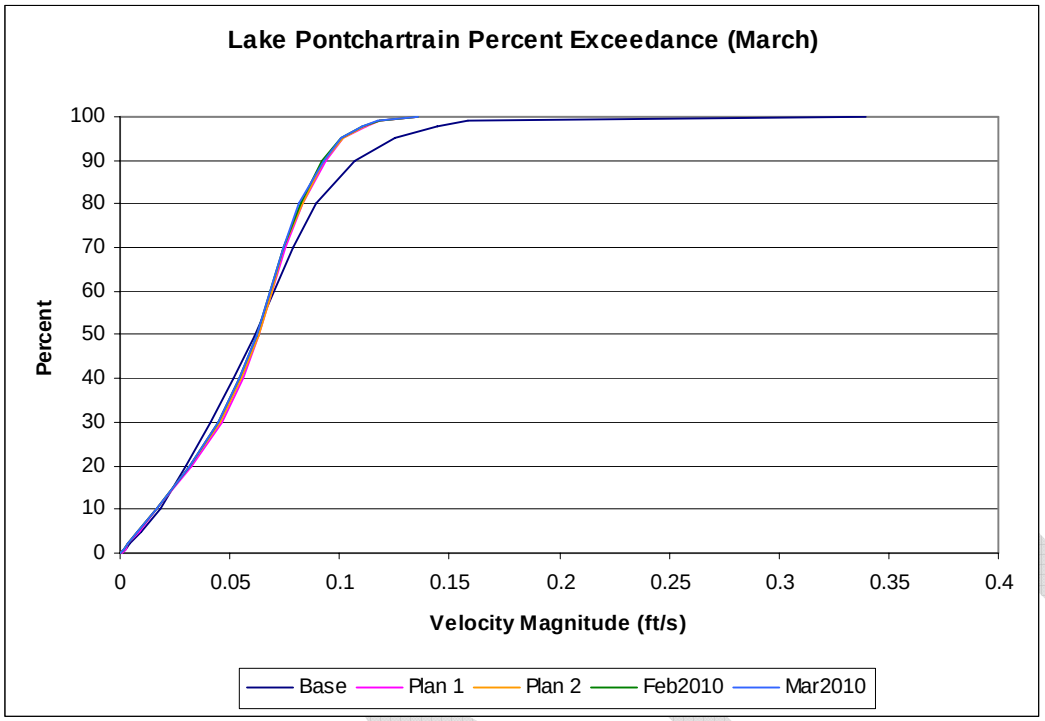

Figure 4-23. Lake Pontchartrain percent exceedance plot for March

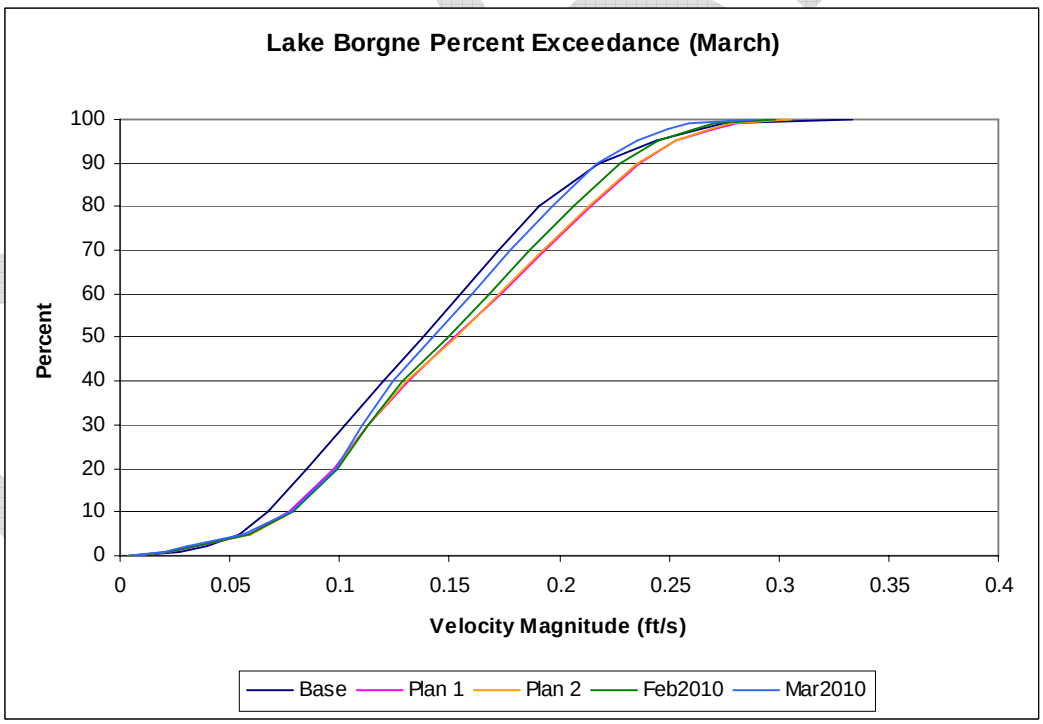

Figure 4-24. Lake Borgne percent exceedance plot for March

The same patterns are seen in the percent exceedance analysis as in the analysis of velocity averages and extremes. The February 2010 plan generates increases in velocity at the GIWW barge gate but decreases at Seabrook. The March 2010 plan, however, reduces the velocity at the GIWW barge gate back to the values obtained with Plan 2. There are small changes in flow in Lake Pontchartrain and Lake Borgne, but the velocity values in these areas are less than or equal to the Plan 1 and Plan 2 values from the previous work. The same trends are observed for both the September 2007 and March 2008 analysis periods.

Water Surface Analysis

A water surface elevation analysis is performed at a total of 16 points within the model domain. The initial locations are set at 250 ft to each side of a proposed structure. Six additional locations are chosen so that an overall response to the system due to the plan alternatives can be observed. Figures 4-25 and 4-26 show the analysis locations. Locations for each side of a structure are shown as a single point. This analysis is performed on both the September and March flow conditions. The water surface elevation for each location and alternative is shown in Figures 4-27 to 4-58. These figures display 12.5 days of the simulation (August 22 – September 3, 2007; March 9 - 21, 2008).

DRAFT

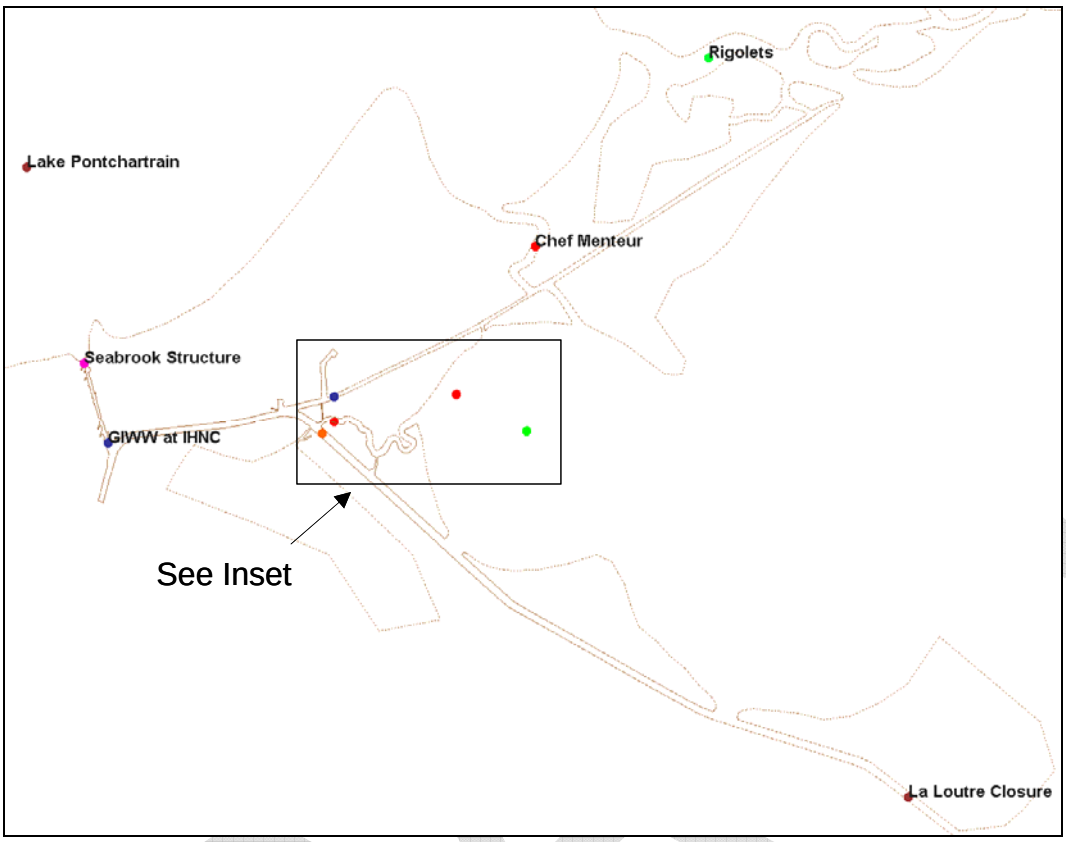

Figure 4-14. Location map for water surface analysis

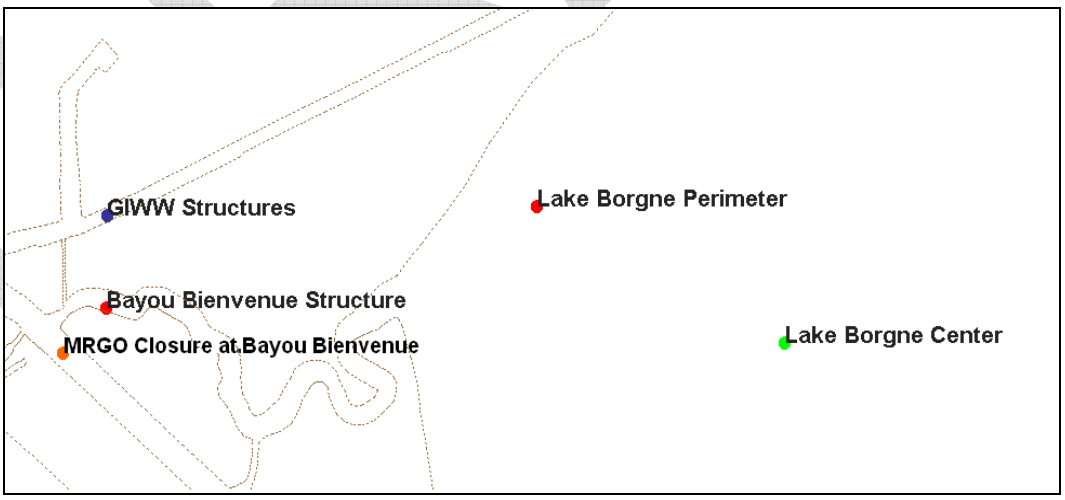

Figure 4-15. Inset for water surface analysis location map

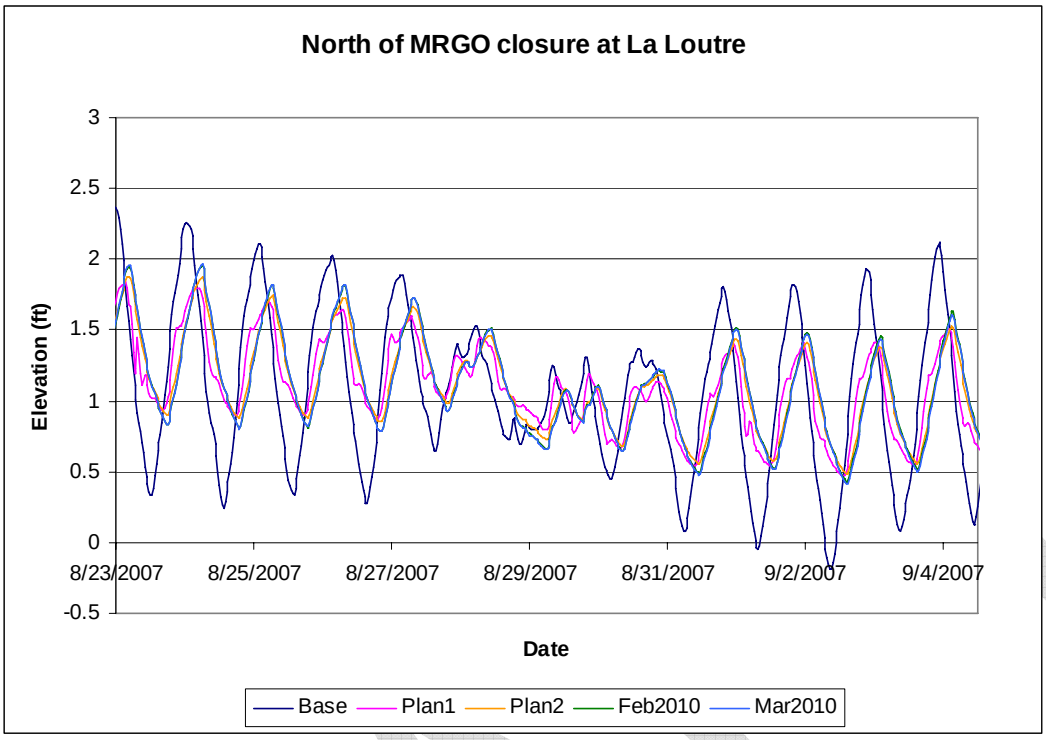

Figure 4-16. Water surface elevation north of MRGO closure at La Loutre (September)

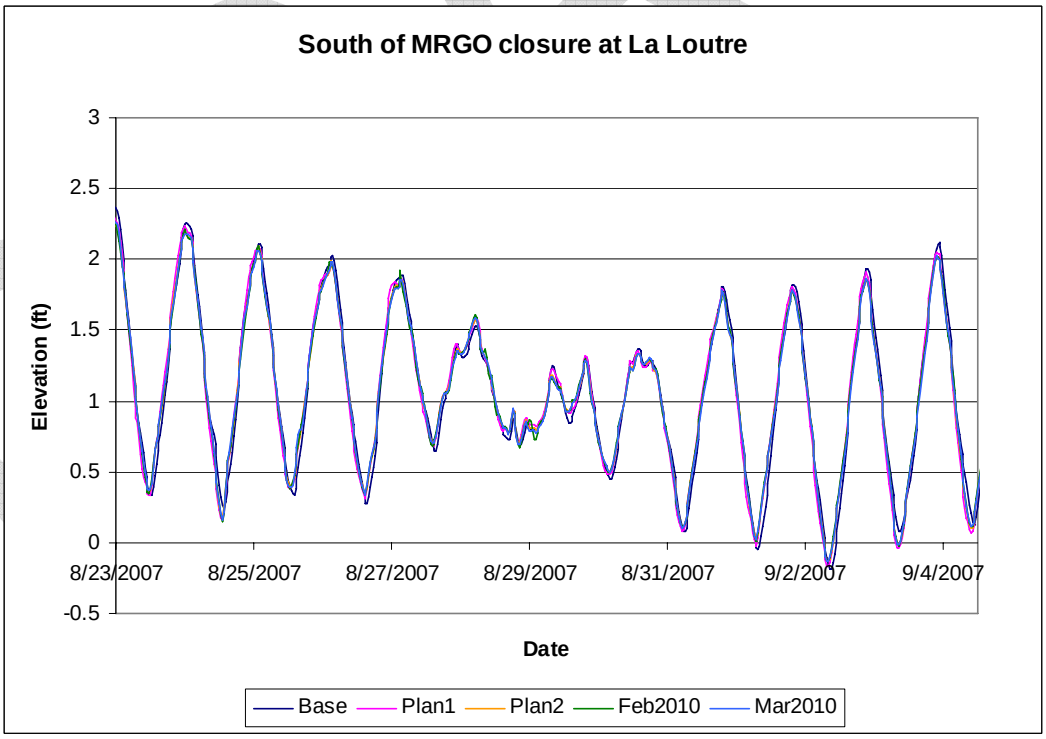

Figure 4-17. Water surface elevation south of MRGO closure at La Loutre (September)

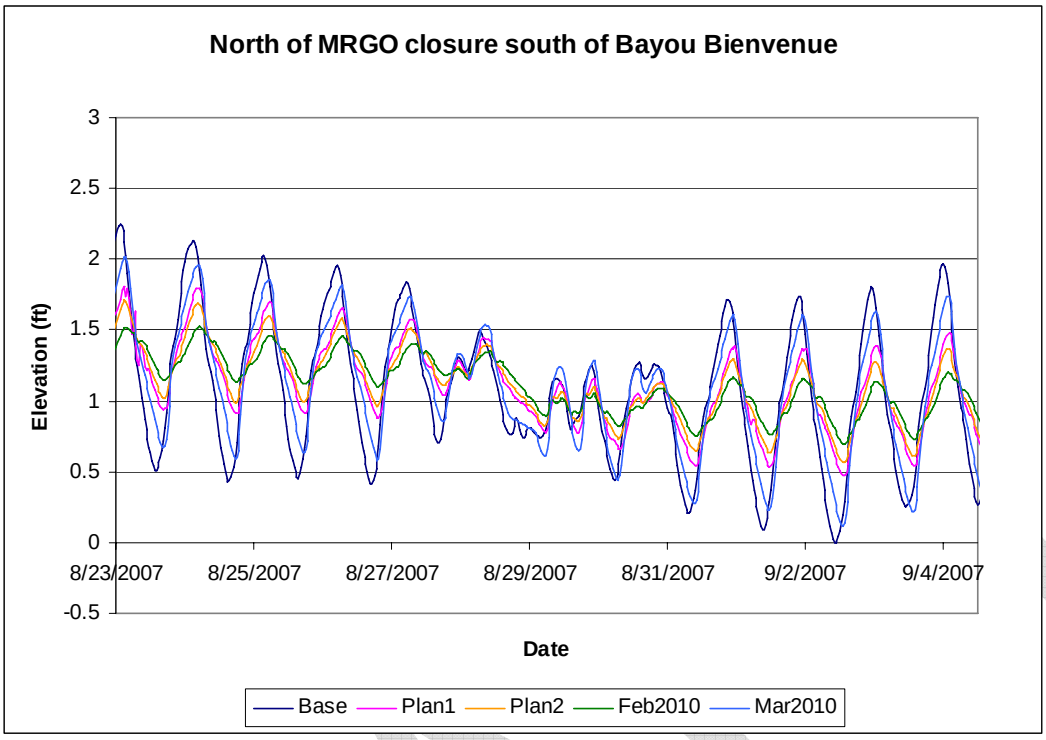

Figure 4-18. Water surface elevation north of MRGO closure at Bayou Bienvenue (September)

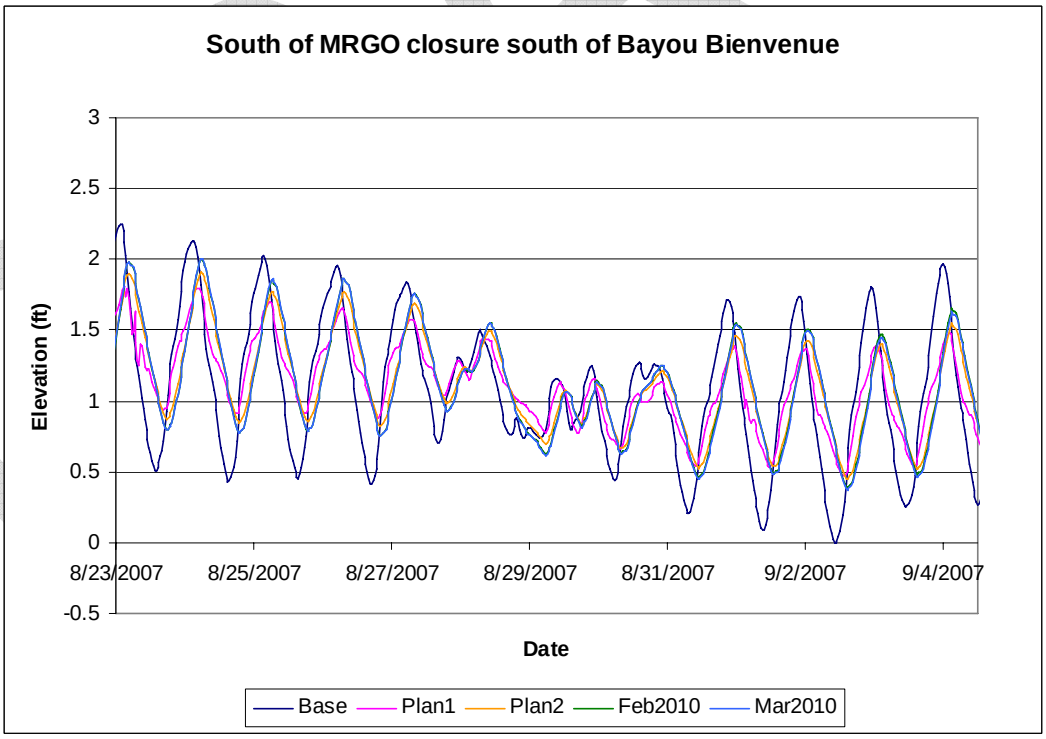

Figure 4-19. Water surface elevation south of MRGO closure at Bayou Bienvenue (September)

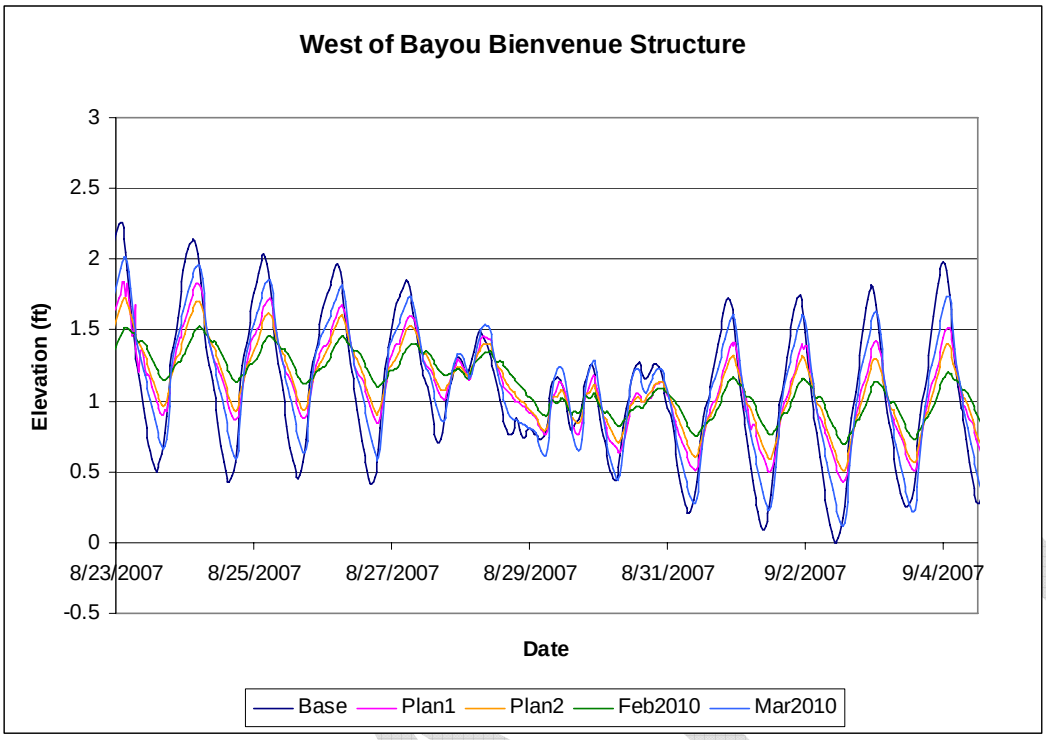

Figure 4-20. Water surface elevation west of Bayou Bienvenue structure (September)

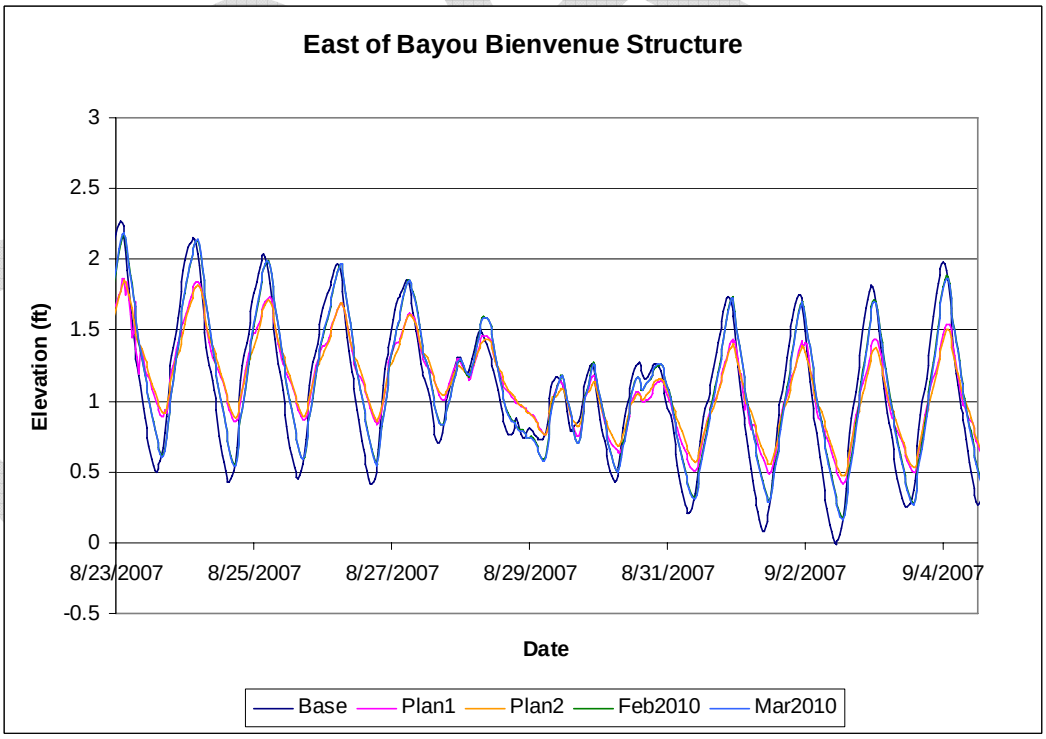

Figure 4-21. Water surface elevation east of Bayou Bienvenue structure (September)

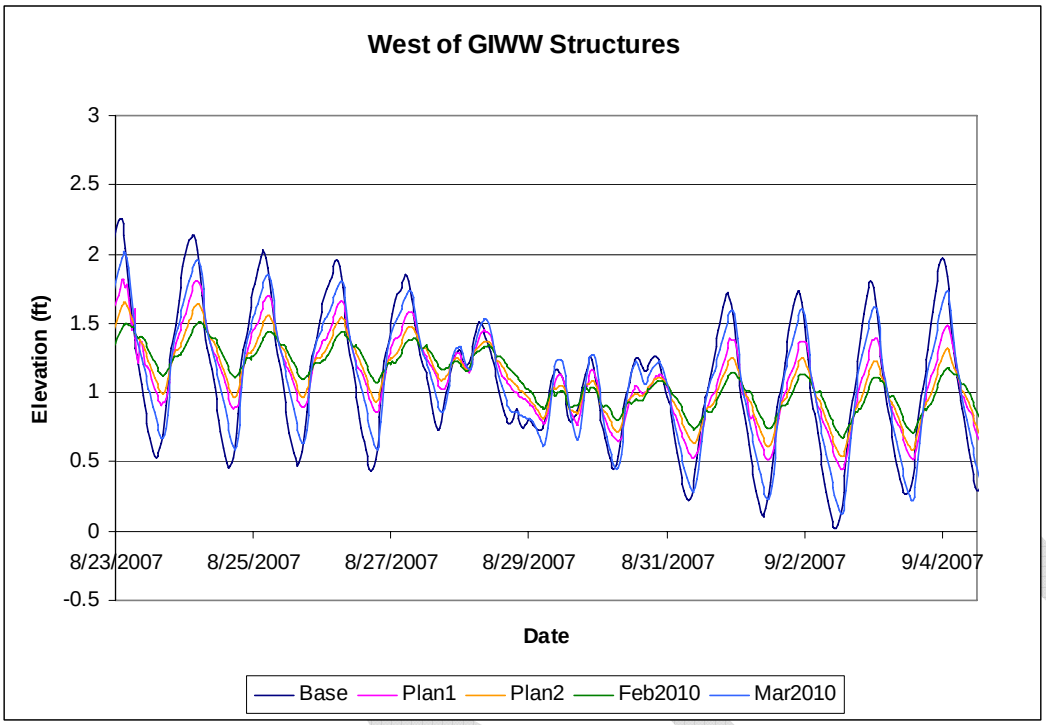

Figure 4-22. Water surface elevation west of GIWW structures (September)

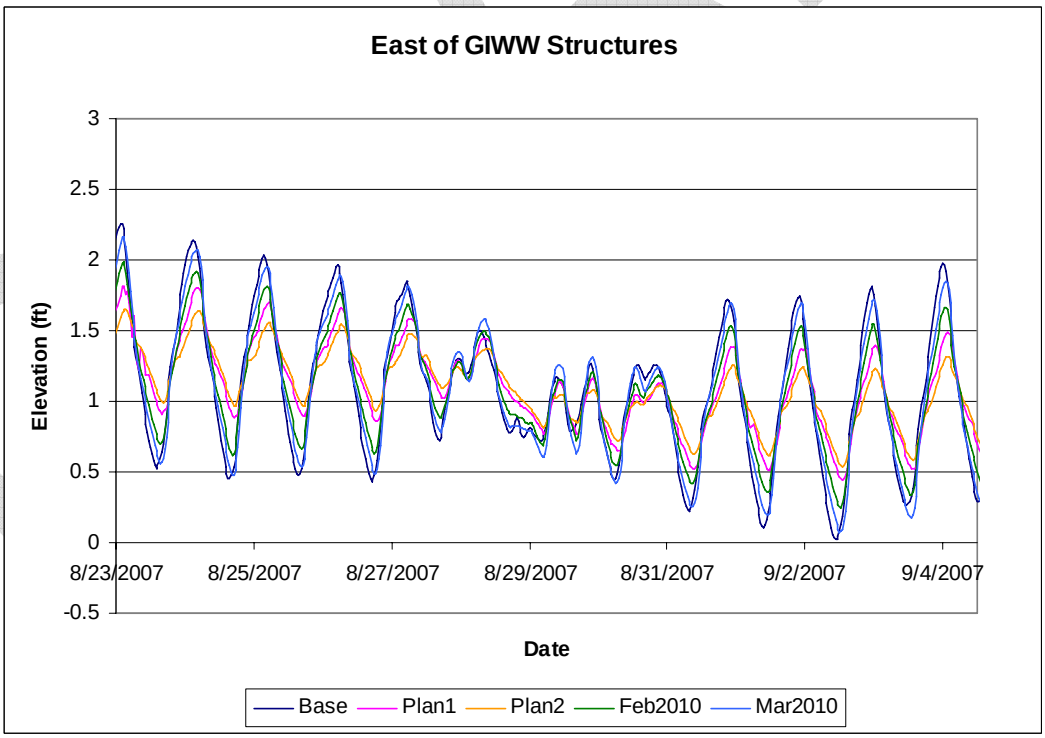

Figure 4-23. Water surface elevation east of GIWW structures (September)

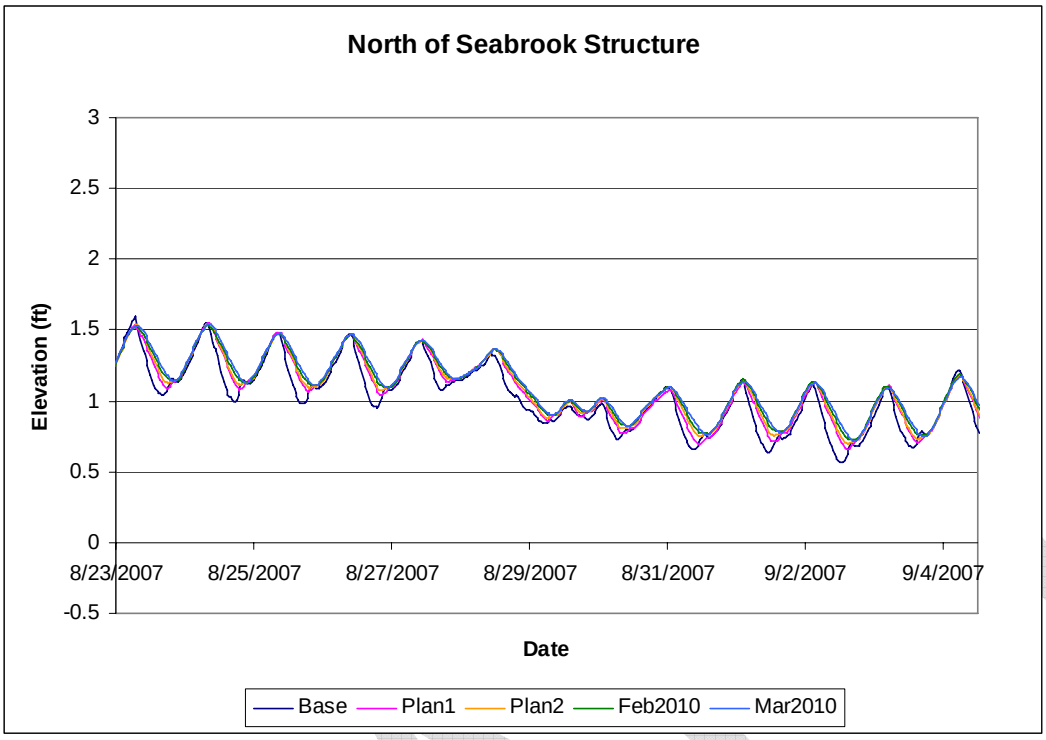

Figure 4-24. Water surface elevation north of Seabrook structure (September)

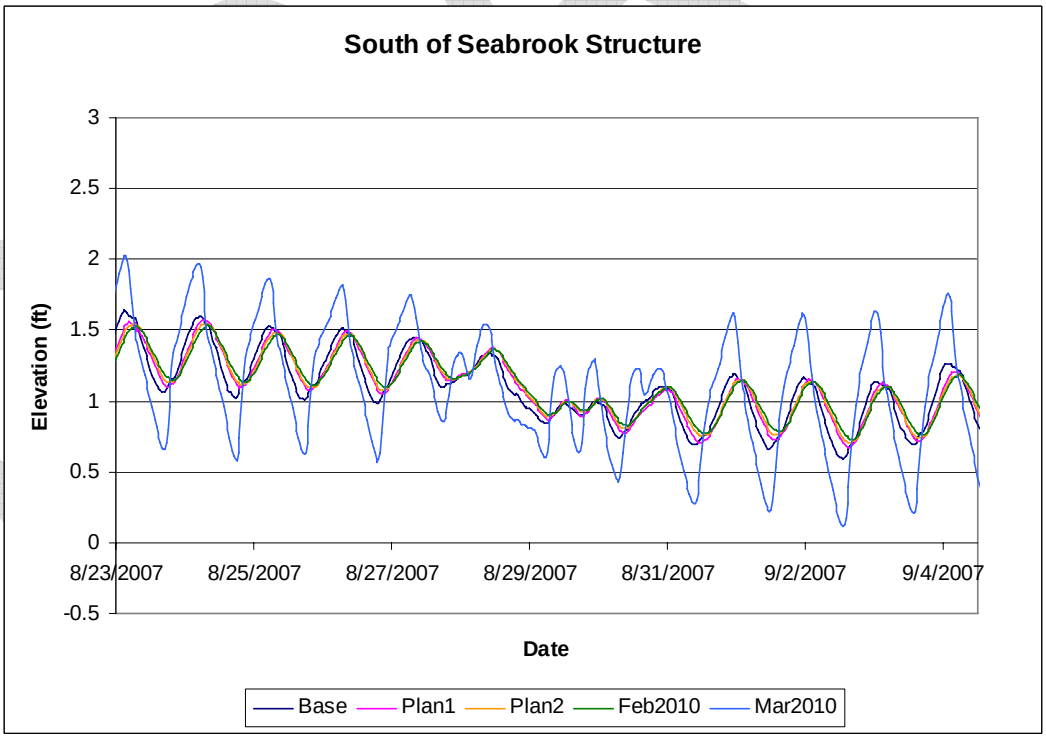

Figure 4-25. Water surface elevation south of Seabrook structure (September)

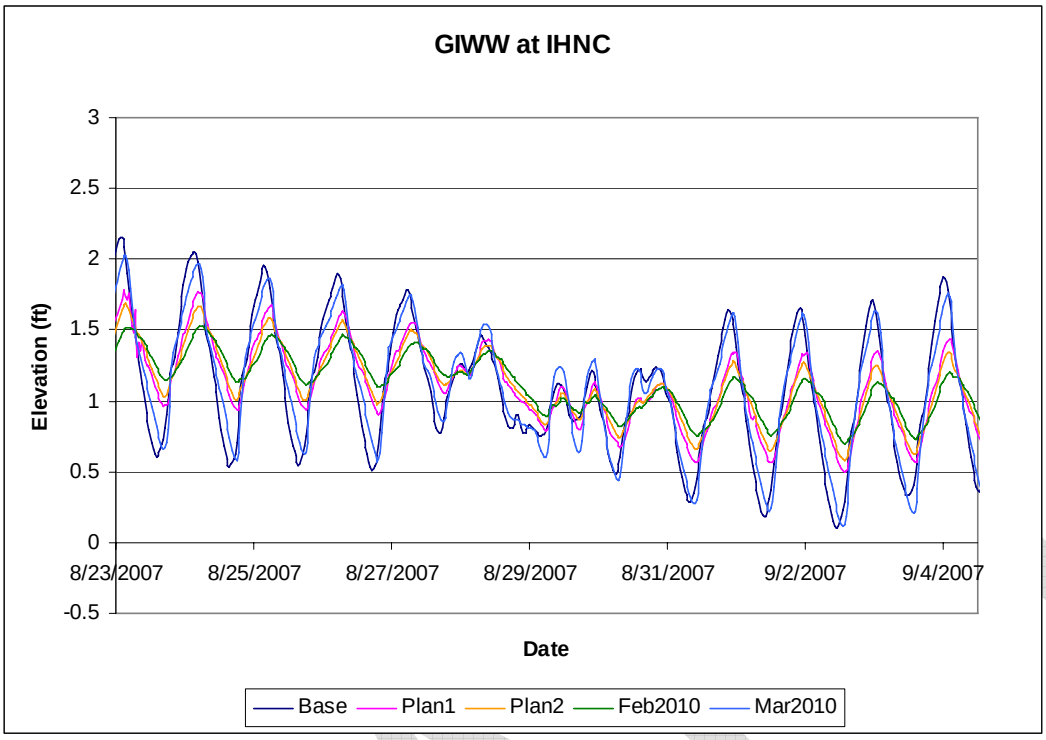

Figure 4-26. Water surface elevation in GIWW at IHNC (September)

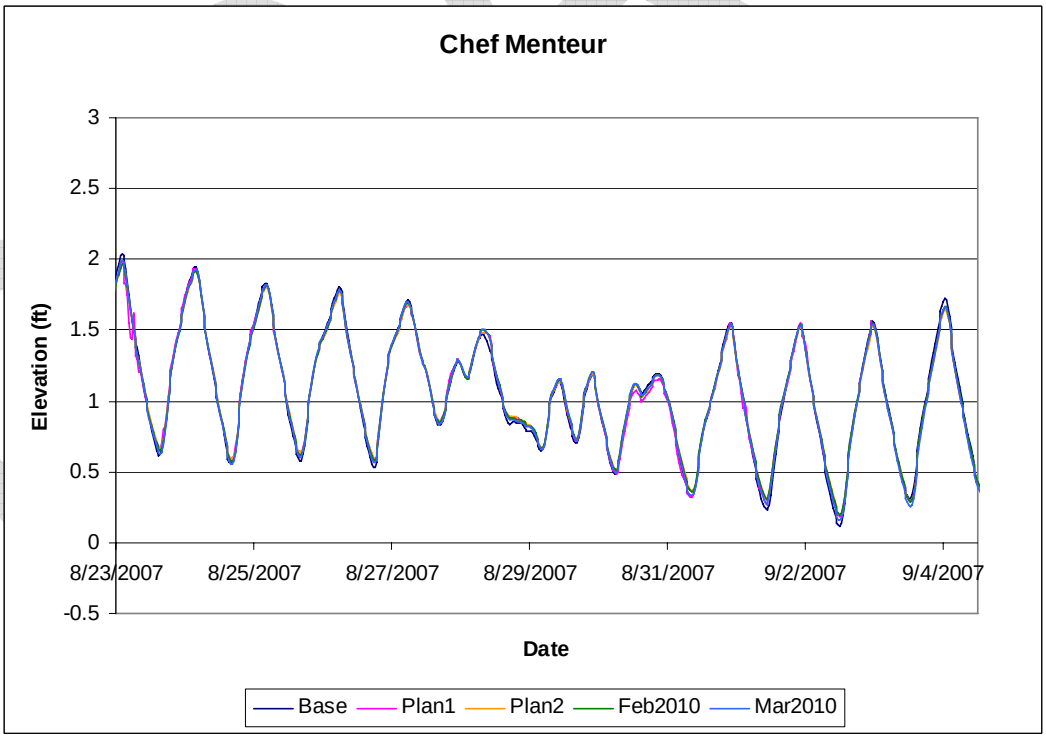

Figure 4-27. Water surface elevation in Chef Menteur (September)

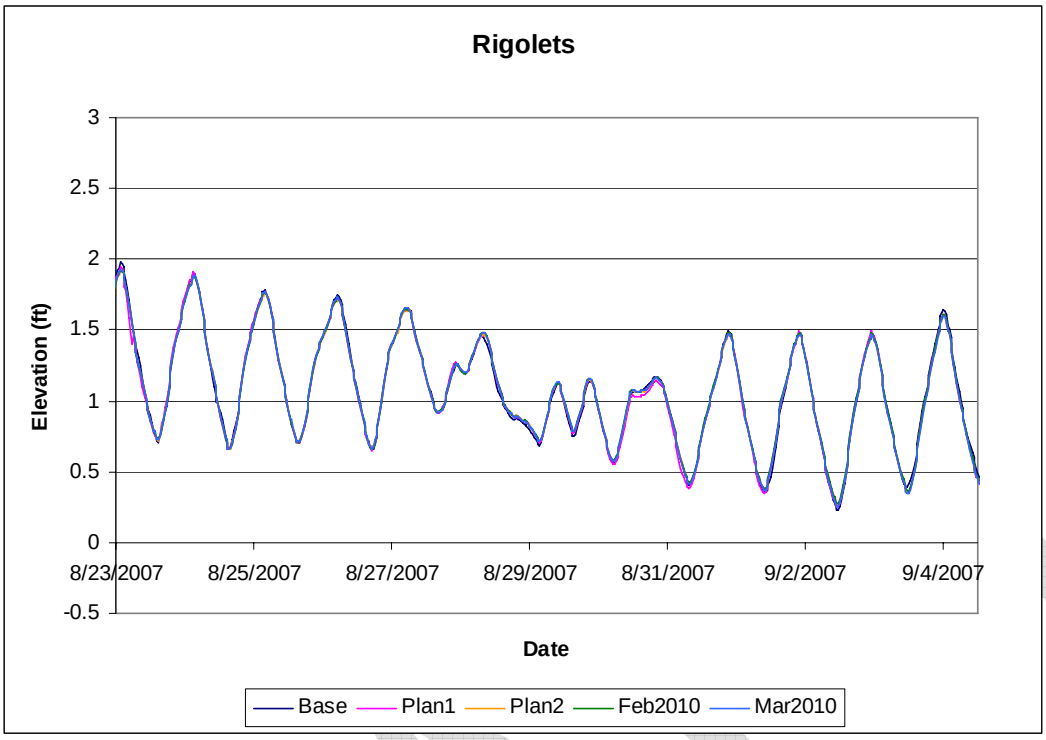

Figure 4-28. Water surface elevation north in Rigolets (September)

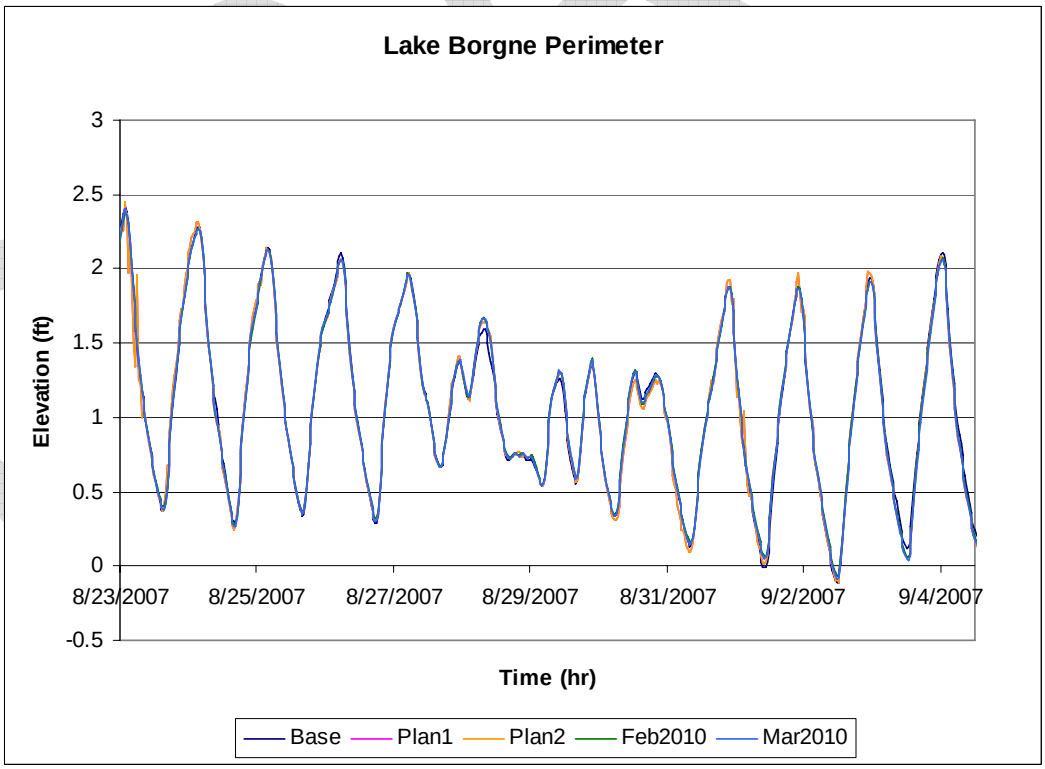

Figure 4-29. Water surface elevation at Lake Borgne perimeter (September)

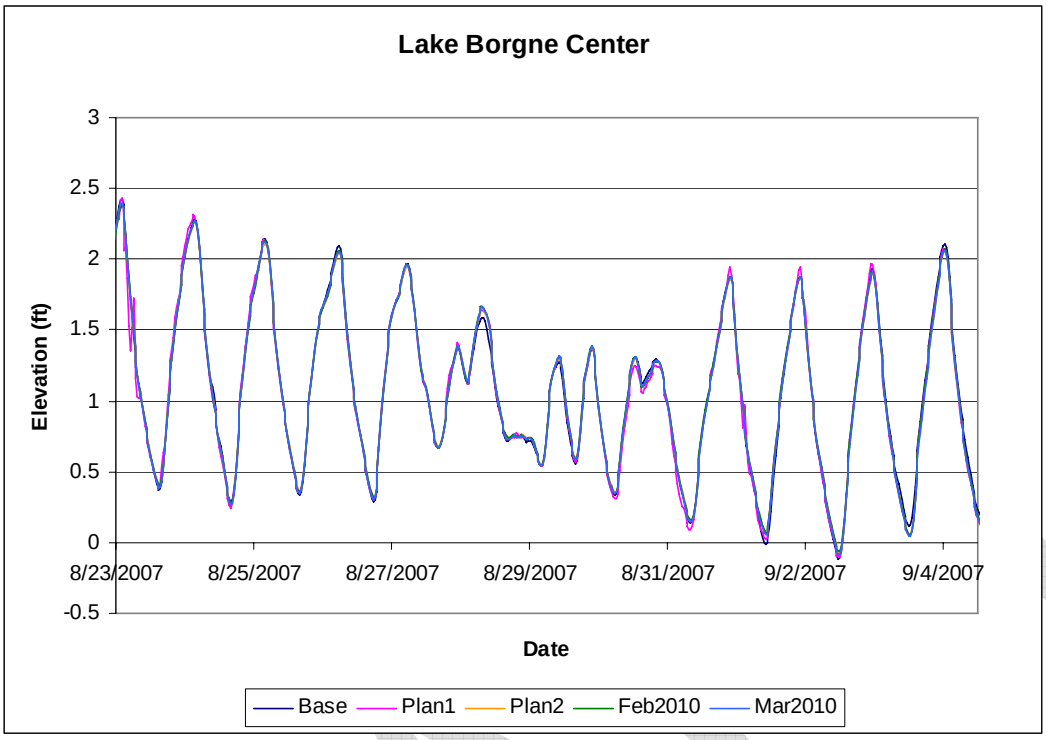

Figure 4-30. Water surface elevation at Lake Borgne center (September)

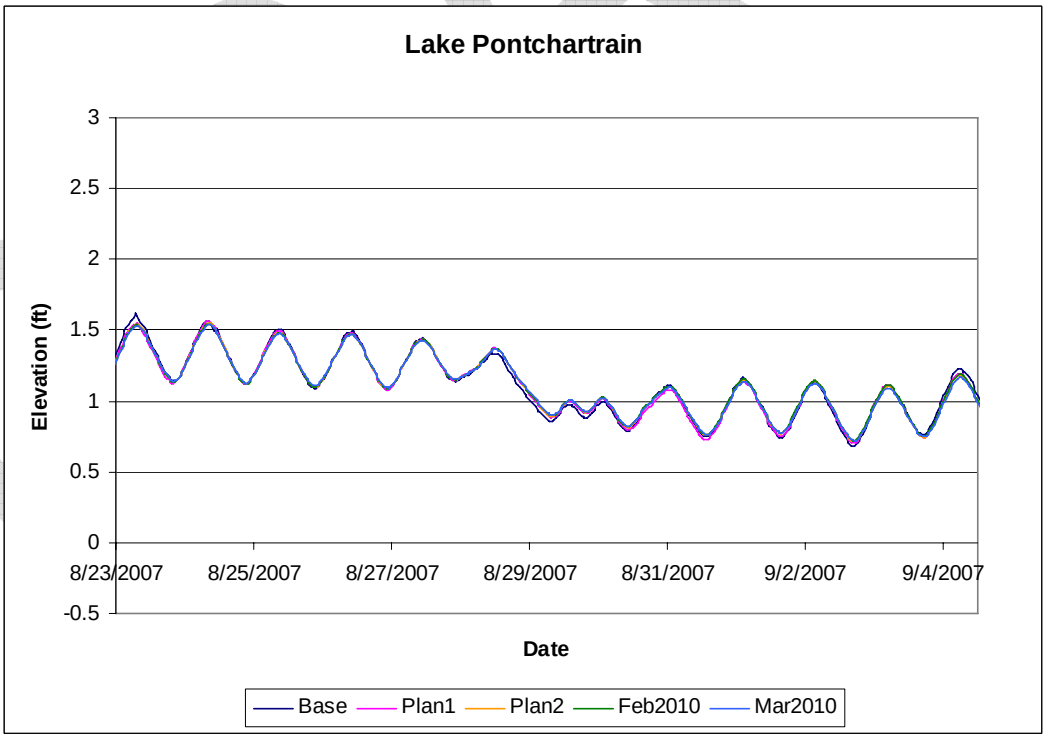

Figure 4-31. Water surface elevation at Lake Pontchartrain (September)

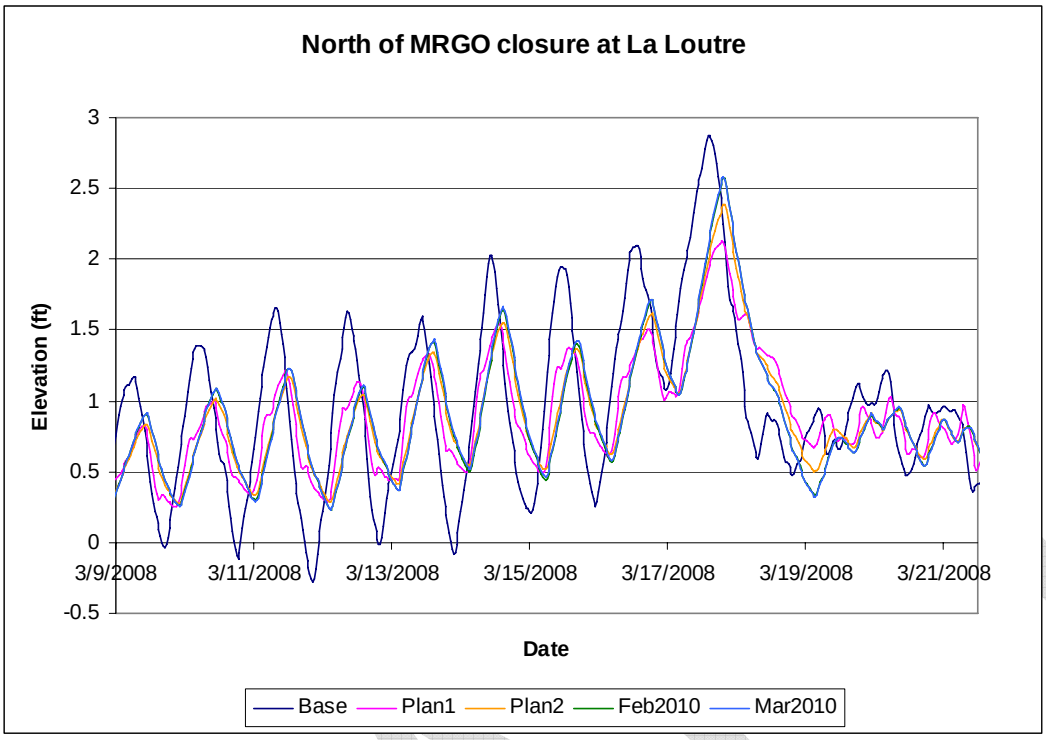

Figure 4-32. Water surface elevation north of MRGO closure at La Loutre (March)

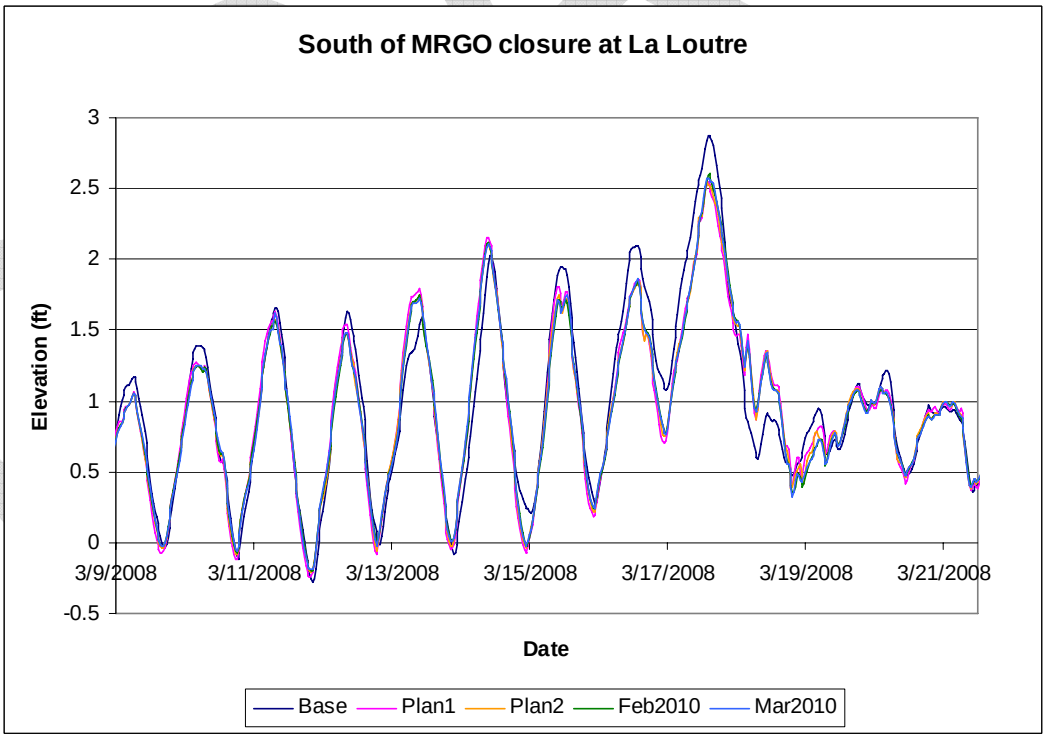

Figure 4-33. Water surface elevation south of MRGO closure at La Loutre (March)

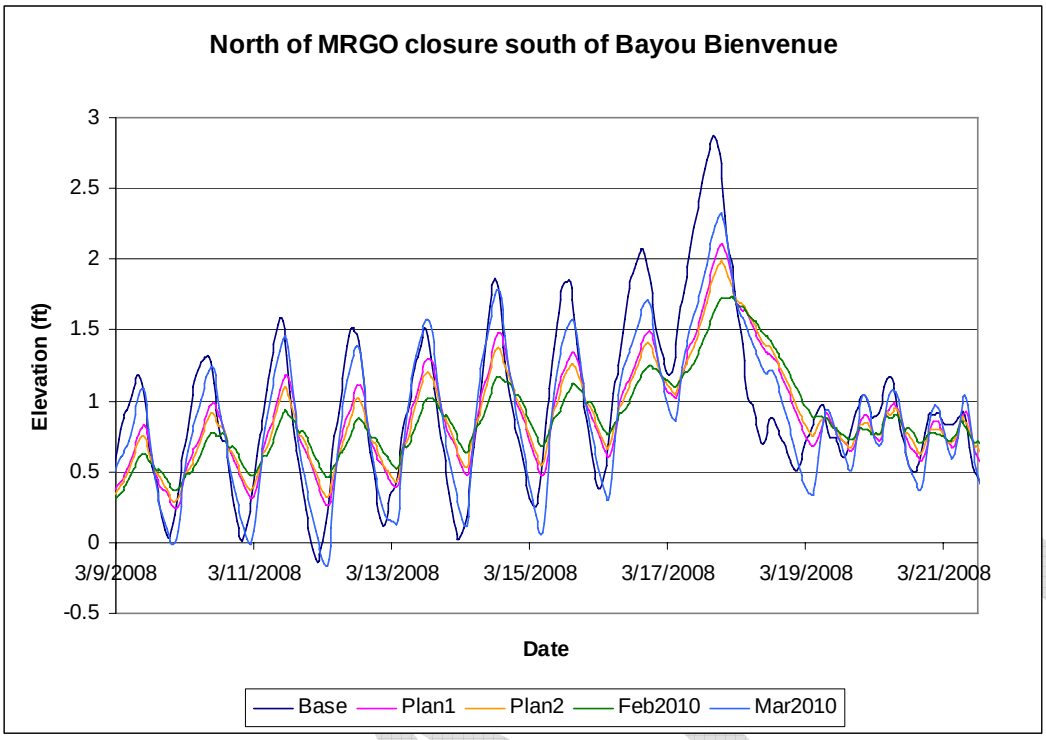

Figure 4-34. Water surface elevation north of MRGO closure at Bayou Bienvenue (March)

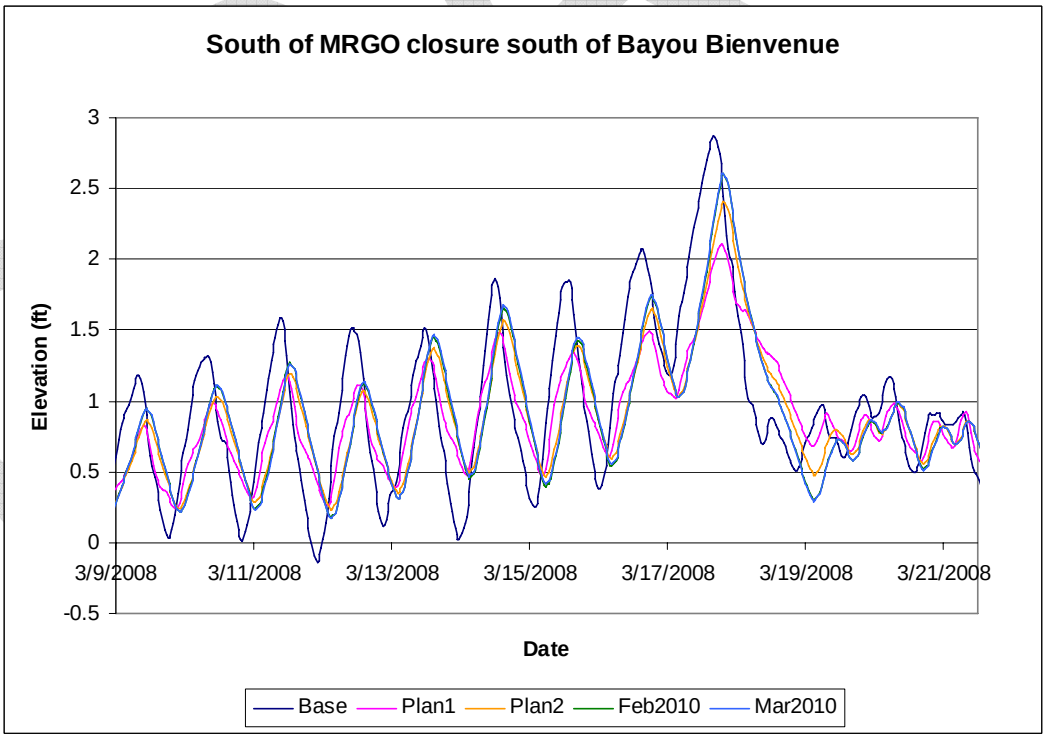

Figure 4-35. Water surface elevation south of MRGO closure at Bayou Bienvenue (March)

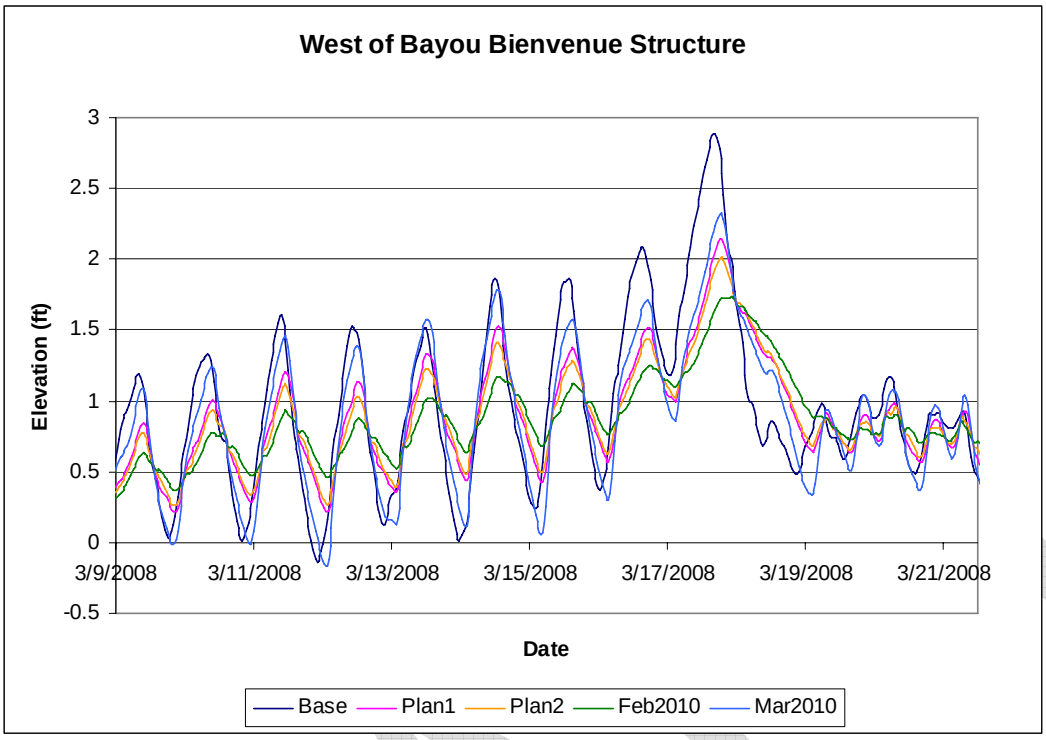

Figure 4-36. Water surface elevation west of Bayou Bienvenue structure (March)

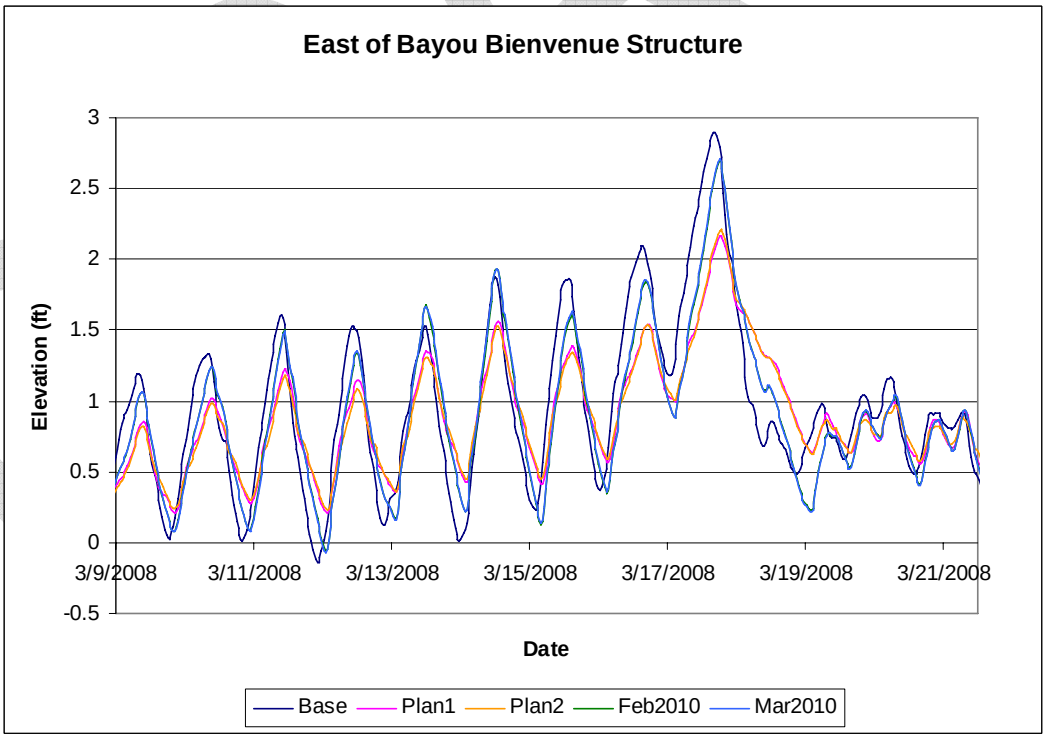

Figure 4-37. Water surface elevation east of Bayou Bienvenue structure (March)

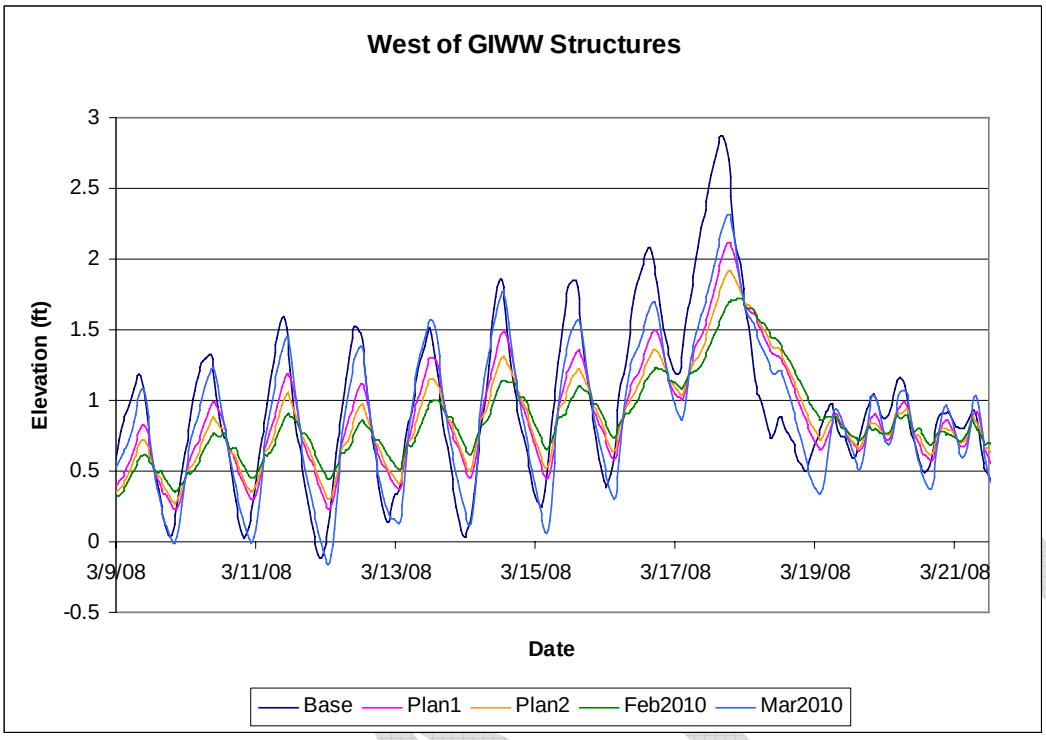

Figure 4-38. Water surface elevation west of GIWW structures (March)

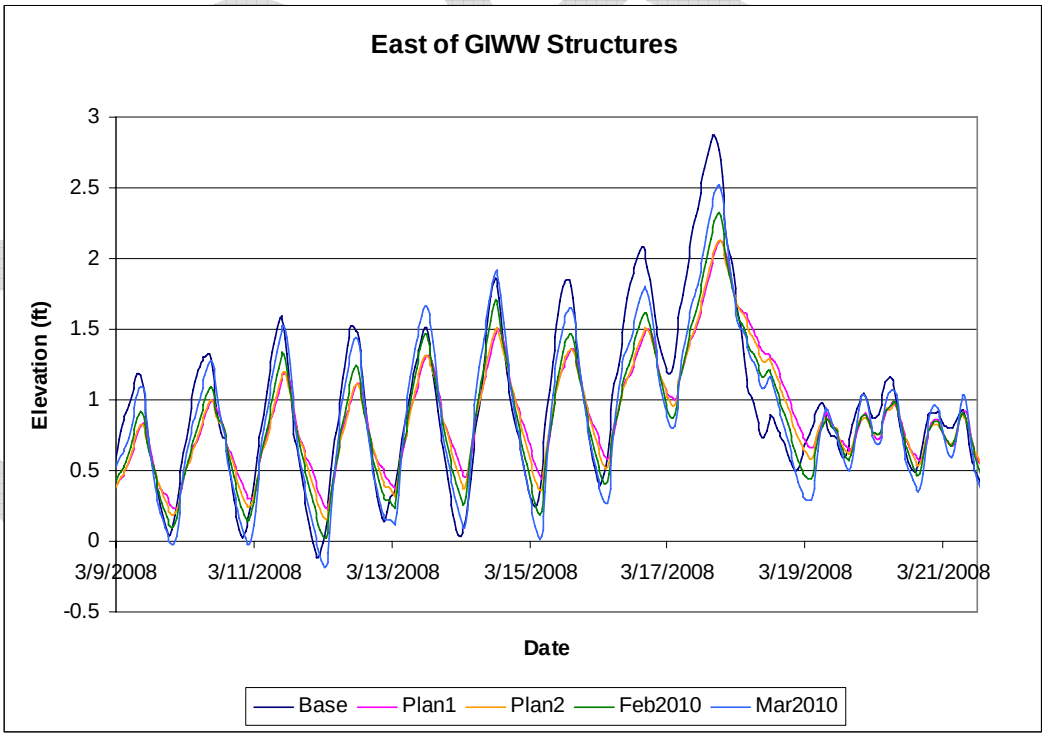

Figure 4-39. Water surface elevation east of GIWW structures (March)

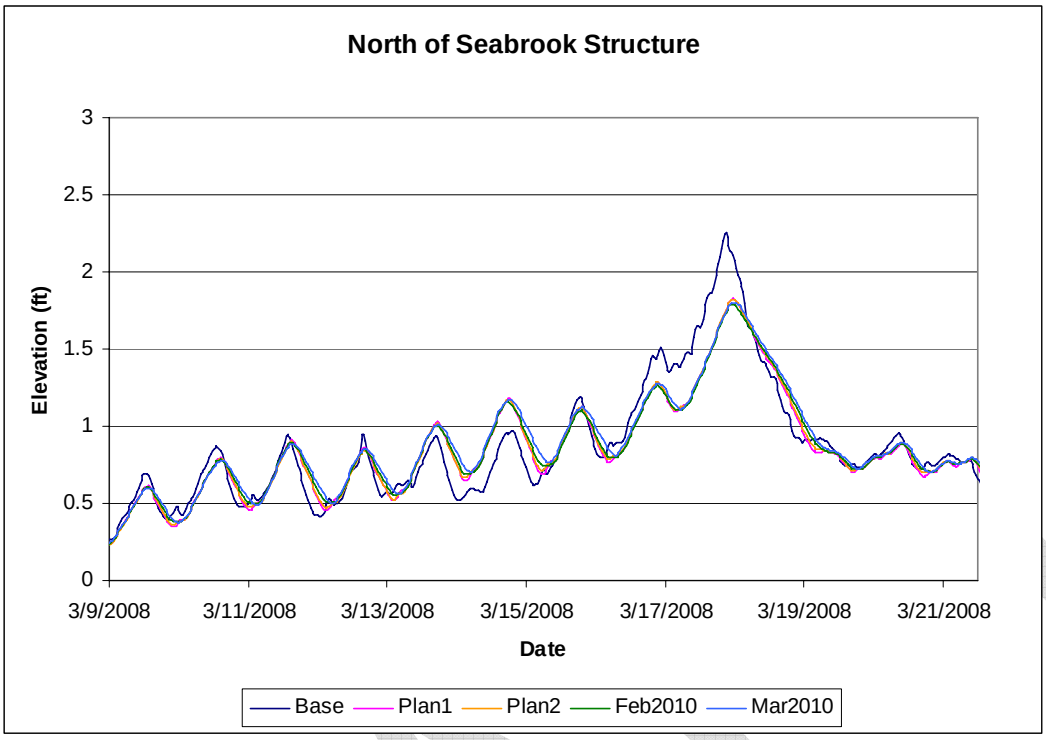

Figure 4-40. Water surface elevation north of Seabrook structure (March)

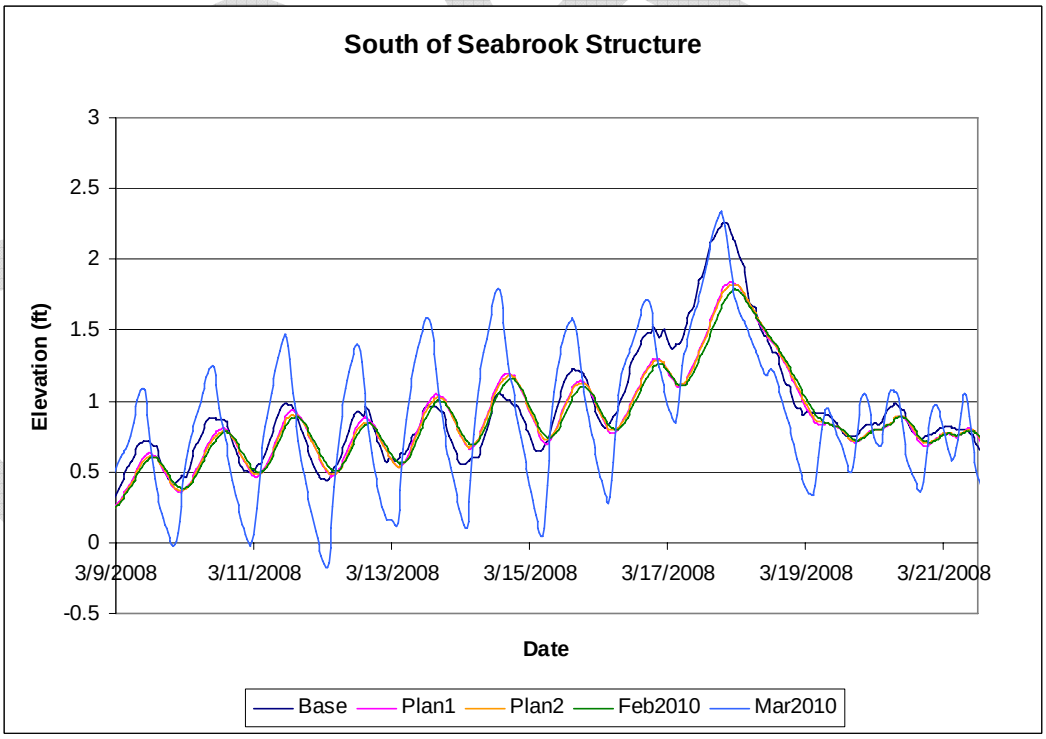

Figure 4-41. Water surface elevation south of MRGO Seabrook structure (March)

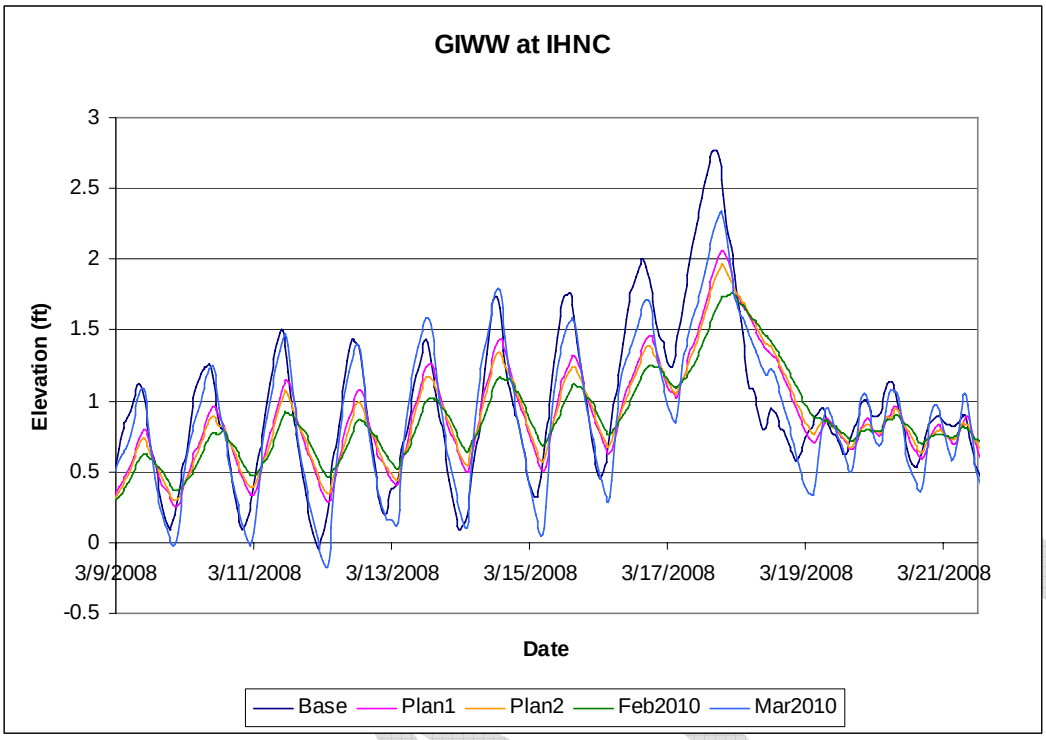

Figure 4-42. Water surface elevation in GIWW at IHNC (March)

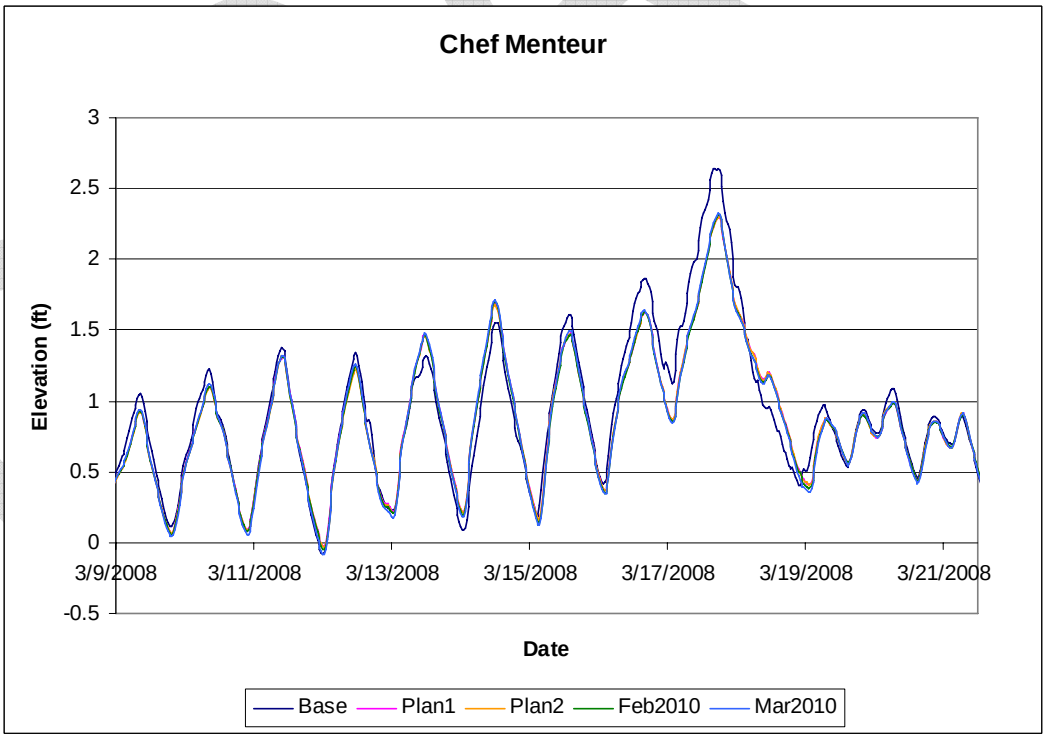

Figure 4-43. Water surface elevation in Chef Menteur (March)

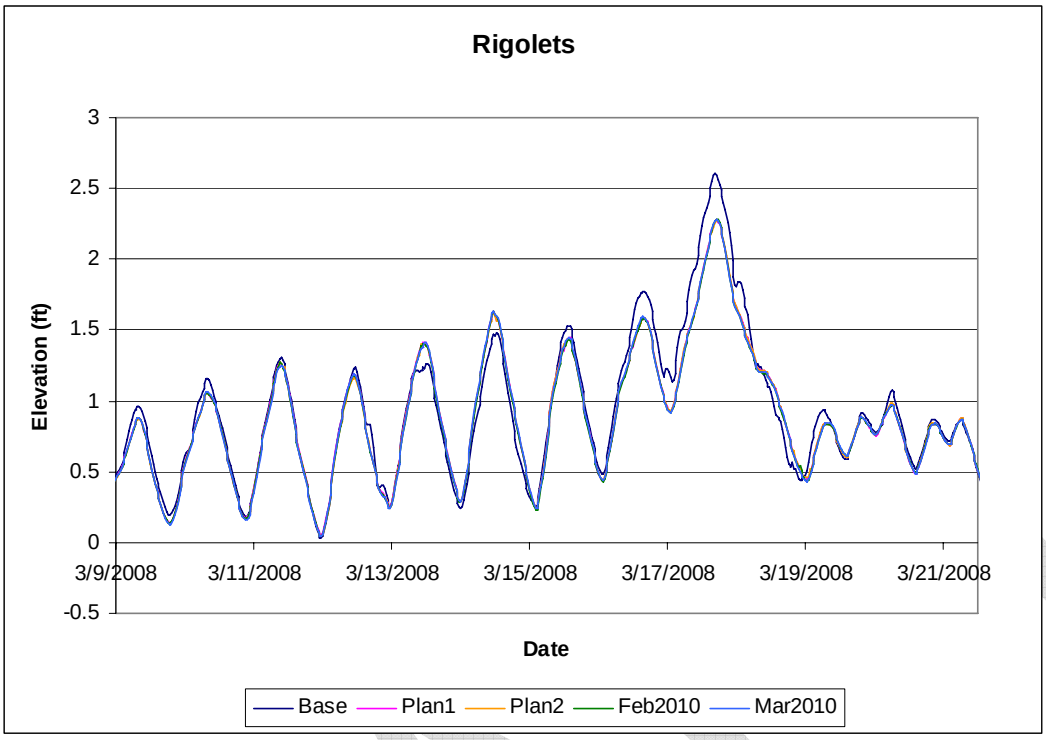

Figure 4-44. Water surface elevation in Rigolets (March)

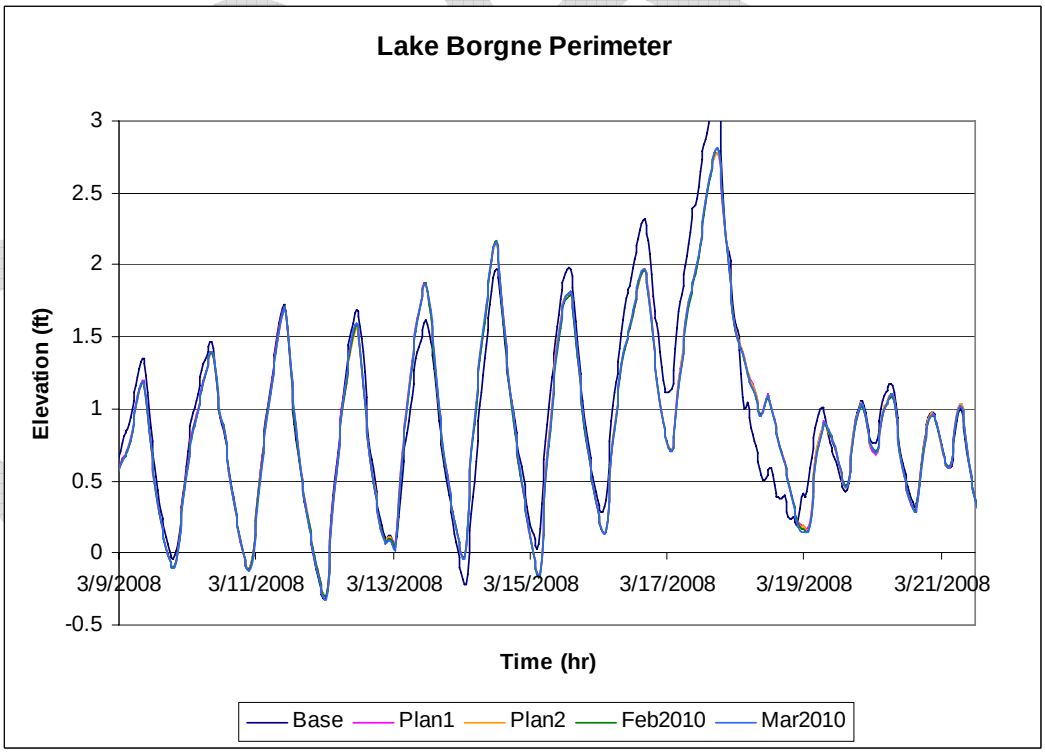

Figure 4-45. Water surface elevation at Lake Borgne perimeter (March)

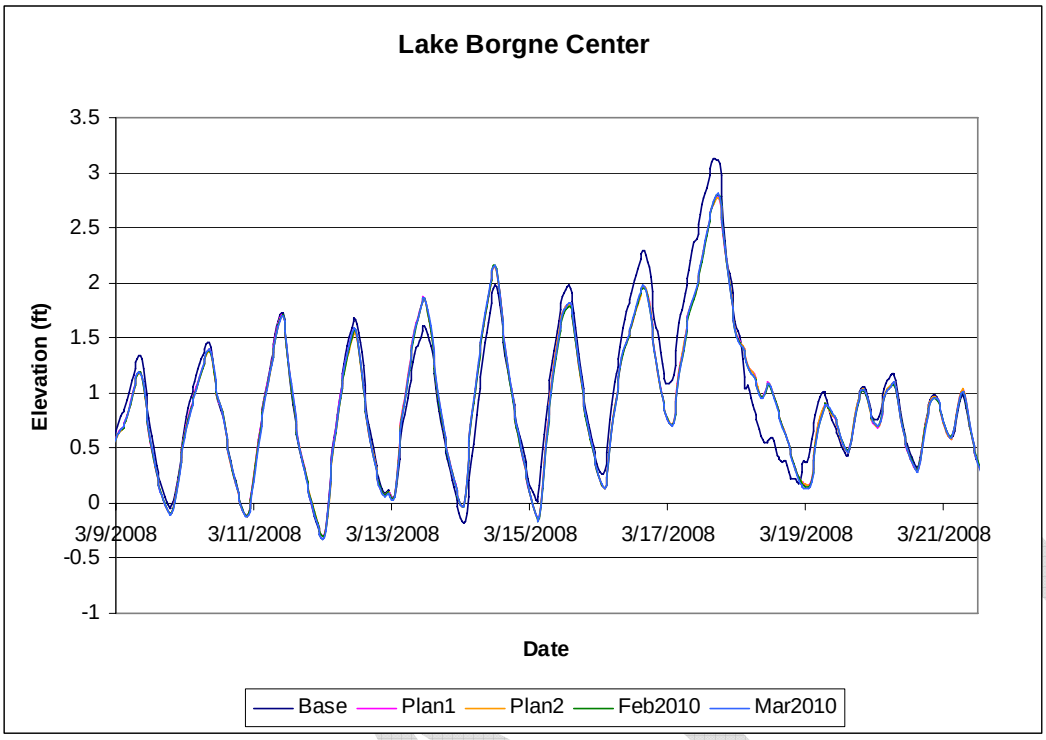

Figure 4-46. Water surface elevation at Lake Borgne center (March)

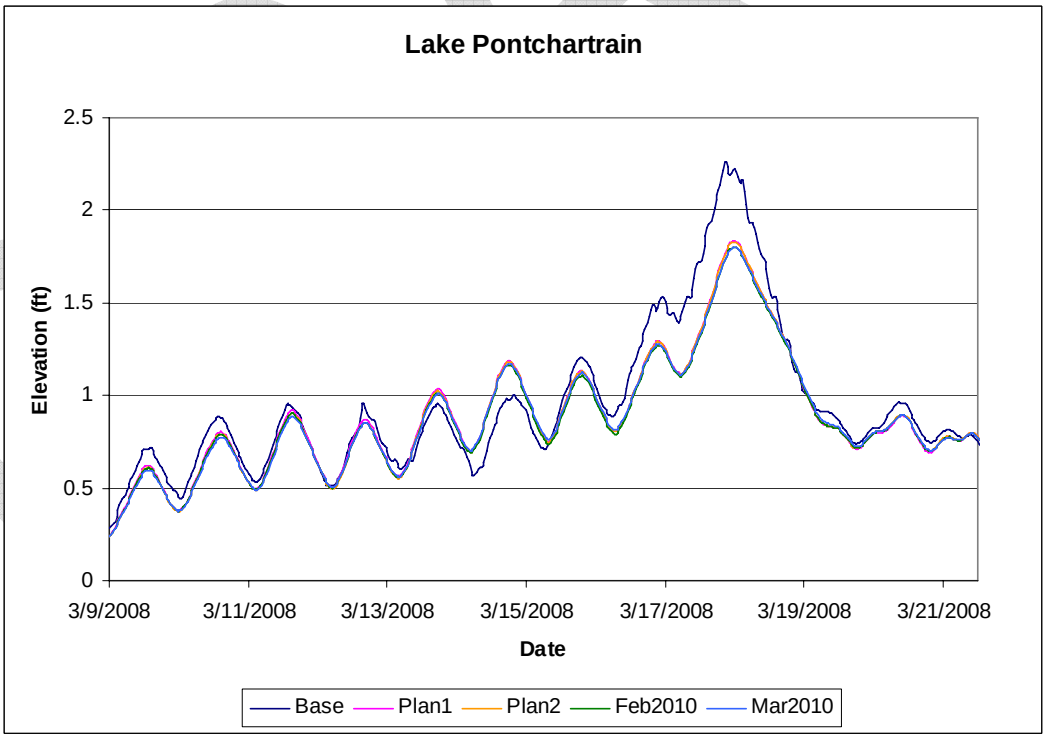

Figure 4-47. Water surface elevation in Lake Pontchartrain (March)

The water surface analysis indicates that there is very little change from the previous plan results for both construction sequence plans at the locations in Lake Borgne, Lake Pontchartrain, Chef Menteur, Rigolets, and locations surrounding the MRGO closure at La Loutre. However, this is not the case at locations in the area of the closures. For all water surface analyses, the same results are evident for both the September 2007 and March 2008 simulation periods.

At the MRGO closure south of Bayou Bienvenue, the southern location is essentially the same as that for Plan 2. At the northern location, however, the February 2010 plan shows a large drop in the range. Since there is a cofferdam at the Bayou Bienvenue structure in this plan, there is less flow into this area. Also, the flow through the GIWW is allowed to exit the area at Seabrook under this plan. The March 2010 plan shows very different results given that a cofferdam is in place at Seabrook. With this plan there is no flow through Seabrook, so all of the flow exchange through the GIWW is getting forced into a limited space, generating an increased range of water surface on the west side of Bayou Bienvenue.

On the western side of the cofferdam at the Bayou Bienvenue structure, the February 2010 plan again indicates a reduction in water level range while the March 2010 plan shows an increase. On the eastern side of this structure the results are the same for both construction sequence plans. Since this structure has a cofferdam for both and the effects of the plans do not extend into Lake Borgne, this similarity is a logical result. At this location, these plans generate an increase in range from the Plan 1 and Plan2 conditions, yet the range is still less than that for the Base condition.

The western side of the GIWW structures shows similar results to those on the west side of the Bayou Bienvenue structure, although in this case only part of the channel is closed. By having a cofferdam at Seabrook (March 2010), the water surface elevation increases between Seabrook and the GIWW structures due to Lake Pontchartrain no longer having an effect on the water surface elevations at this location and the only path of flow being through the GIWW barge gate. On the eastern side of the GIWW structures, both plans produce an increase in the water surface elevation range. The values for the March 2010 plan are greater than those for the February 2010 plan, although the March 2010 values do not exceed those from the original Base condition.

DRAFT

The effects of these construction sequence plans at the Seabrook locations are such that the location north of the structure experiences little change. This is due to the large area at this location in the Lake. There is a small reduction in the low end water level values, but this change is small. South of the structure, however, there is a large increase in the water level when the pathway is closed. The March 2010 plan indicates amplifications of the flows reaching this location on the order of 50%. Seabrook was the only outlet for the wave traveling the GIWW, so now that this pathway is blocked, the tide is stopped at this location. The February 2010 plan does not experience this effect since the flow entering the GIWW can still pass through Seabrook. For this plan, there is actually a slight drop in water surface at the southern Seabrook location.

One analysis location lies between the GIWW structures and Seabrook. At this location where the GIWW meets the IHNC, the same general pattern is evident. The February 2010 plan generates a decrease in the water surface elevation range and the March 2010 plan generates an increase. There is a slight shift in phase for the March 2010 condition as well due to the complete blockage at Seabrook. The drop in range for February 2010 is due to the limitation of the flow volume through the GIWW barge gate.

Circulation Changes

For all of these analyses, the driving factor is the pathway through which flow is allowed. The February 2010 plan only allows flow from Lake Borgne to pass through the 150 ft wide GIWW barge gate and then into Lake Pontchartrain at Seabrook. No flow is able to travel up the MRGO or into the area through Bayou Bienvenue since both pathways are blocked. The March 2010 plan further limits the transport pathways by allowing flow exchange through the GIWW barge gate with no exit at Seabrook. The only means for exchange into Lake Pontchartrain is through Chef Menteur and the Rigolets. Therefore all flow entering the GIWW and IHNC is limited to exiting the system in the same manner, through a single 150 ft structure. Figures 4-48 and 4-49 illustrate the circulation patterns. The yellow lines indicate locations where the pathways are blocked due to construction.

DRAFT

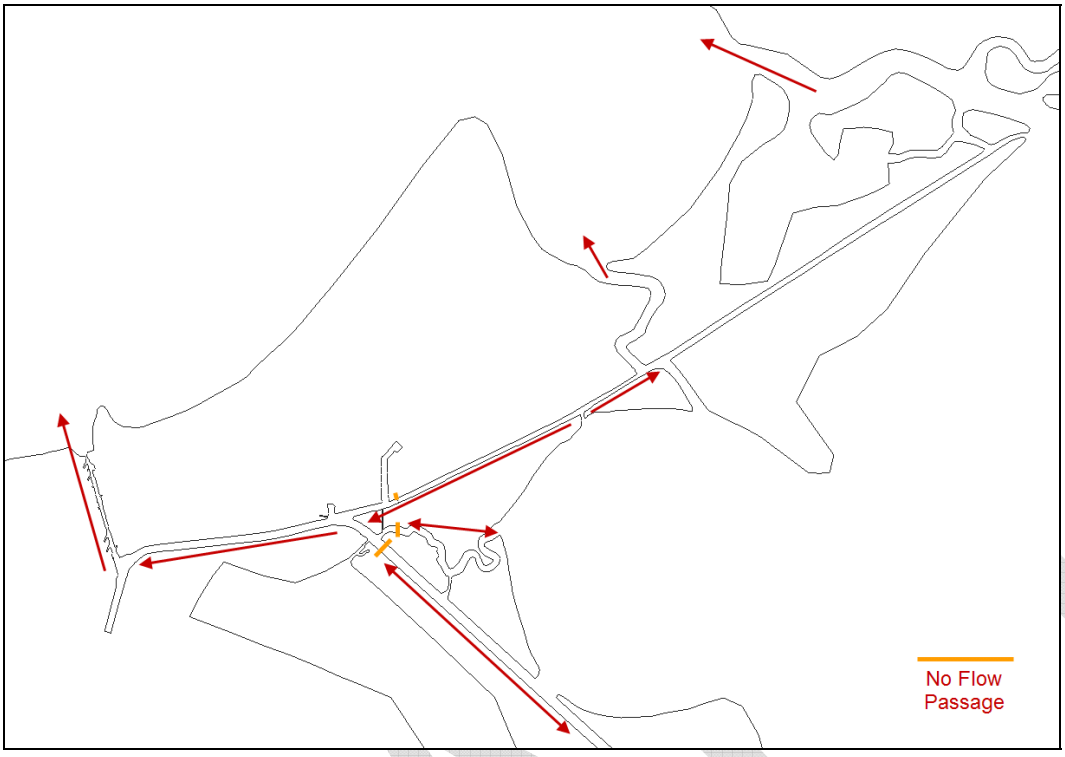

Figure 4-48. February 2010 plan circulation

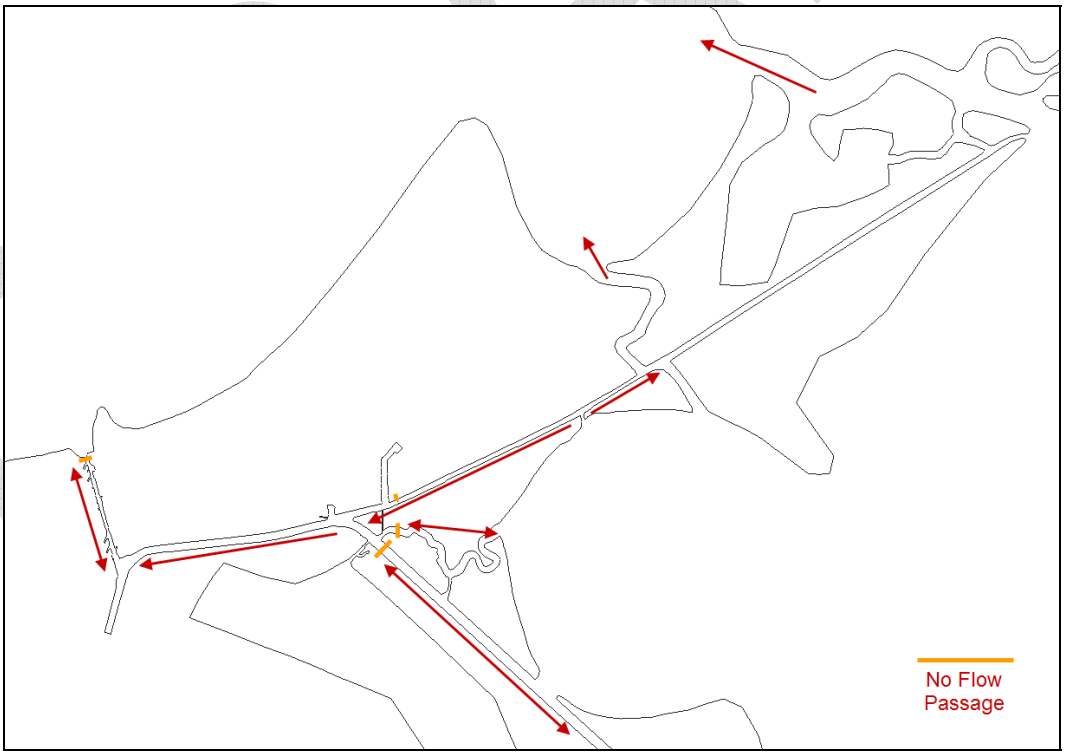

Figure 4-49. March 2010 plan circulation

5 Conclusions

The work presented in this report documents hydrodynamic modeling and analysis of two construction sequence plans which will occur during the construction of the Borgne alignment and Seabrook structures included in the HSDRRS. This plan will allow for improved protection of the city of New Orleans, Louisiana as well as surrounding areas. Previous research focused on the changes that these structures would generate on the flows and fish transport. Research is also being performed to analyze the effects these changes have on navigation. This report specifically focuses on the construction sequence plans during which the Bayou Bienvenue structure and GIWW sector gate are being built as well as the construction of the Seabrook structure. The February 2010 plan includes cofferdams on the Bayou Bienvenue and at the GIWW sector gate in addition to closing the MRGO at La Loutre and south of Bayou Bienvenue. The March 2010 plan adds a cofferdam at Seabrook.

Water surface elevation, velocity magnitude and direction, and percent exceedance analyses were performed at several locations within the model domain, focusing on the areas likely to be affected by the plan changes. The average velocity values are given in Table 1. The results of the model simulations indicate that these construction sequence plans generate changes to water surface elevations and velocity magnitudes and flow patterns in the vicinity of the system changes. These plans do not generate measurable changes in Lake Pontchartrain or Lake Borgne. At the GIWW barge gate, the February 2010 changes to velocity are much larger than the March changes and may impact navigation through this structure. At Seabrook, the February 2010 plan decreases the velocity magnitudes since less flow is entering the system due to the constriction on the GIWW.

Table 1. Average velocity values at the GIWW and Seabrook structures for the base and each construction sequence plan during both analysis periods

Average Velocity (ft/s)	Base				Feb 2010				Mar 2010			
	Positive		Negative		Positive		Negative		Positive		Negative	
	Sept	Mar	Sept	Mar	Sept	Mar	Sept	Mar	Sept	Mar	Sept	Mar
GIWW	0.2	0.2	-0.2	-0.1	2.9	3.0	-2.8	-3.1	1.8	1.5	-1.7	-1.6
Seabrook	2.4	2.7	-2.4	-2.6	0.9	1.1	-0.9	-1.1	0.0	0.0	0.0	0.0

DRAFT

Water surface elevations are effected in a different manner. The February 2010 plan reduces the water surface elevation range at most locations when compared to the plan condition that includes the Borgne alignment (Plan 2). However, the March 2010 plan increases the water surface elevation ranges in the locations confined by the closures. By limiting the pathways by which the tidal range can travel, flow is limited and can get trapped and amplified within the system. The magnitude of these changes should be considered when determining the operating procedures during the planned construction sequence.

DRAFT

References

McAnally, W.H., and Berger, R.C. (1997). "Salinity Changes in Pontchartrain Basin Estuary Resulting from Bonnet Carre` Freshwater Diversion," Technical Report CHL-97-2, U.S. Army Waterways Experiment Station, Vicksburg, MS.

Tate, J.N., Carrillo, A.R., Berger, R.C., and Thibodeaux, B.J. (2002). "Salinity Changes in Pontchartrain Basin Estuary, Louisiana, Resulting from Mississippi River-Gulf Outlet Partial Closure Plans with Width Reduction," Technical Report CHL-TR-02-12, U.S. Army Engineer Research and Development Center, Vicksburg, MS.

Tate, Jennifer N., Lackey, Tahirih C., and McAlpin, Tate O. (2009). "Seabrook Fish Larval Transport Study," Technical Report in review, U.S. Army Engineer Research and Development Center, Vicksburg, MS.

DRAFT

Appendix: Description of the Adaptive Hydraulics Model (ADH)

ADH is a state-of-the-art Adaptive Hydraulics Modeling system developed by the Coastal and Hydraulics Laboratory. It is capable of simulating both saturated and unsaturated groundwater, overland flow, three-dimensional Navier-Stokes flow, and two- or three-dimensional shallow water problems with the current study utilizing the two-dimensional shallow water module. The 2D shallow-water equations used for this application are a result of the vertical integration of the equations of mass and momentum conservation for incompressible flow under the hydrostatic pressure assumption. Written in conservative form, the 2D shallow water equations are:

$$\frac{\partial \mathbf{U}}{\partial t} + \frac{\partial \mathbf{F}}{\partial x} + \frac{\partial \mathbf{G}}{\partial y} + \mathbf{H} = 0 \tag{1}$$

where

$$\mathbf{U} = \begin{Bmatrix} h \\ uh \\ vh \end{Bmatrix} \tag{2}$$

$$\mathbf{F} = \begin{Bmatrix} uh \\ u^2 h + \frac{1}{2} g h^2 - h \dfrac{\sigma_{xx}}{\rho} \\ uvh - h \dfrac{\sigma_{yx}}{\rho} \end{Bmatrix} \tag{3}$$

DRAFT

$$\mathbf{G} = \begin{Bmatrix} vh \\ uvh - h\dfrac{\sigma_{xy}}{\rho} \\ v^2 h + \frac{1}{2} g h^2 - h\dfrac{\sigma_{yy}}{\rho} \end{Bmatrix} \tag{4}$$

and

$$\mathbf{H} = \begin{Bmatrix} 0 \\ gh\dfrac{\partial z_b}{\partial x} + n^2 gh\dfrac{u\sqrt{u^2+v^2}}{C_o h^{1/3}} \\ gh\dfrac{\partial z_b}{\partial y} + n^2 gh\dfrac{v\sqrt{u^2+v^2}}{C_o h^{1/3}} \end{Bmatrix} \tag{5}$$

where:

ρ = fluid density

g = gravitational acceleration

z_b = riverbed elevation

n = Manning's roughness coefficient

h = flow depth

u = x-component of velocity

v = y-component of velocity

DRAFT

C_o = dimensional conversion coefficient (1 for SI units, 1.486 for U.S. customary units)

σ's = the Reynolds stresses due to turbulence, where the first subscript indicates the direction, and the second indicates the face on which the stress acts.

The Reynolds stresses are determined using the Boussinesq approach to the gradient in the mean currents.

$$\sigma_{xx} = 2\rho v_t \frac{\partial u}{\partial x} \tag{6}$$

$$\sigma_{yy} = 2\rho v_t \frac{\partial v}{\partial y} \tag{7}$$

and

$$\sigma_{xy} = \sigma_{yx} = 2\rho v_t \left(\frac{\partial u}{\partial y} + \frac{\partial v}{\partial x} \right) \tag{8}$$

where v_t = kinematic eddy viscosity (which varies spatially).

The ADH shallow-water equations are placed in conservative form so that mass balance and the balance of momentum and pressure are identical across an interface. This is important in order to match the speed and height of a surge or hydraulic jump.

The equations are represented in a finite element approach. The quality of the numerical solution depends on the choice of the basis/trial function and the test function. The trial function determines how the variables are represented and the test function determines the manner in which the differential equation is enforced. In the Galerkin approach the test functions

DRAFT

are chosen to be identical with the trial functions. When the flow is advection-dominated, the Galerkin approach produces oscillatory behavior. The Galerkin form of the test function cannot detect the presence of a node-to-node oscillation and so allows this spurious solution. The approach used in ADH is to enrich the standard Galerkin test function with an additional term that can detect and control this spurious solution.

The Petrov-Galerkin method used here is based on elemental constants for coefficients. This reduces the stabilization to the nonconservative form. This is not a problem since the stabilization is only applied within the elements and uses the Galerkin test function to enforce "flux" balance across element edges. For illustration, consider the shallow-water equations in nonconservative form

$$\frac{\partial U}{\partial t} + A\frac{\partial U}{\partial x} + B\frac{\partial U}{\partial y} + H = 0 \tag{9}$$

where $A = \frac{\partial F}{\partial U}$ and $B = \frac{\partial G}{\partial U}$. The trial functions (or interpolation/basis functions) are the Lagrange polynomials. These are piecewise linear functions that are continuous across element boundaries. Spatial derivatives, however, are not continuous across these element edges. Each of the dependent and independent variables is interpolated via these trial functions. For example,

$$\tilde{u}(x) = \sum_{j=1}^{N} \phi_j(x) u_j , \tag{10}$$

means that the approximate solution is made up of the product of the trial function for node j and the nodal value at that location. The test function is chosen as:

$$\phi_i^* = \phi_i I + \alpha \left(\frac{\partial \phi_i}{\partial x} A + \frac{\partial \phi_i}{\partial y} B \right)$$

(11)

where,

$$\alpha = 0.5 l \left[\bar{v} \bullet \bar{v} + gh + \left(\frac{l}{\Delta t} \right)^2 \right]^{-1/2}$$

(12)

l	=	$(\Omega_e)^{1/2}$, the square of the element area
$\bar{v}$	=	$(\bar{u}, \bar{v})$, the element average velocity components
Δt	=	time step size

The finite element statement becomes:

$$\int_{\Omega} \left(\phi_i \frac{\partial U_l}{\partial t} - \frac{\partial \phi_i}{\partial x} F_l - \frac{\partial \phi_i}{\partial y} G_l + \phi_i H_l \right) d\Omega +$$

$$\int_{\partial\Omega} \phi_i \left\{ F_l n_x + G_l n_y \right\} ds + \sum_e \int_{\Omega_e} \alpha \left(\frac{\partial \phi_i}{\partial x} A_l + \frac{\partial \phi_i}{\partial y} B_l \right)$$

$$\left(\frac{\partial U_l}{\partial t} + A_l \frac{\partial U_l}{\partial x} + B_l \frac{\partial U_l}{\partial y} + H_l \right) = 0 \qquad (13)$$

Where, the subscript l indicates the finite element approximation. The Petrov-Galerkin contributions are integrated on the interior of the elements, but not across element edges. This contribution stabilizes the Galerkin approach. This contribution stabilizes the Galerkin approach. This scheme utilizes a single scaling factor α. This is different from the scheme reported in Berger and Stockstill (1995). That scheme involved

DRAFT

scaling each eigenvalue, but that method does not converge using the iterative solver in ADH. Instead, a single value scaling (Equation 12) is used.

One of the major benefits of ADH is its ability to adapt the mesh in areas where additional resolution is needed to properly resolve the hydrodynamics. This process is done by normalizing the results so that an error quantity is determined for each element. If this error exceeds the tolerance set by the user, then the element is refined. ADH is also able to unrefined previously refined areas when the added resolution is no longer needed. ADH contains other essential features such as wetting and drying, completely coupled sediment transport, and wind effects. A series of modularized libraries make it possible for ADH to include vessel movement, friction descriptions, as well as a host of other crucial features. ADH can run in parallel or on a single processor and runs on both Windows systems and UNIX based systems.

DRAFT